Lithos 132–133 (2012) 162–179

Contents lists available at SciVerse ScienceDirect

Lithos

journal homepage: www.elsevier.com/locate/lithos

The fate of subducted oceanic slabs in the shallow mantle: Insights from boron isotopes and light element composition of metasomatized blueschists from the Mariana forearc

Sonja Pabst [a,*], Thomas Zack [b], Ivan P. Savov [c], Thomas Ludwig [a], Detlef Rost [d], Sonia Tonarini [e], Edward P. Vicenzi [f,1]

[a] Institut für Geowissenschaften, Universität Heidelberg, INF 234–236, 69120 Heidelberg, Germany
[b] Institut für Geowissenschaften, Universität Mainz, Becher-Weg 21, 55099 Mainz, Germany
[c] School of Earth and Environment, University of Leeds, Leeds LS2 9JT, United Kingdom
[d] School of Earth, Atmospheric and Environmental Sciences, University of Manchester, Williamson Building, Oxford Road, Manchester M13 9PL, United Kingdom
[e] Istituto Geoscienze Georisorse, C.N.R. Pisa, Italy
[f] Department of Mineral Sciences, Smithsonian Institution, National Museum of Natural History, Washington D.C. 20560, USA

ARTICLE INFO

Article history:
Received 24 June 2011
Accepted 11 November 2011
Available online 25 November 2011

Keywords:
Blueschist
Izu-Bonin-Marianas subduction zone
Secondary ion mass spectrometry (SIMS)
Time-of-Flight (ToF)-SIMS
Boron isotopes
Mélange

ABSTRACT

Serpentine muds from South Chamorro Seamount (SCS), drilled during ODP Leg 195 at Site 1200 contain metamafic clasts that experienced blueschist-facies metamorphism (including the critical mineral assemblage pumpellyite – Na-amphibole – epidote). These schists represent fragments from the actual slab–mantle interface at ~27 km depth. Their heterogeneous lithology with a metasomatic character indicates significant mobility of major elements in the Mariana forearc, a region of mélange formation as it can also be observed in onland exposures such as the Catalina Schist. As the Mariana forearc blueschists show no late stage alteration they permit the direct study of material transfer during the subduction processes at an active convergent margin.

This study presents the first data of detailed B isotope (δ^{11}B) and light element variations in blueschist-facies minerals from the Mariana arc system. The primary foci are B and Li concentrations and δ^{11}B values analyzed by SIMS and ToF-SIMS techniques. Minerals such as (Na-rich) amphibole, phengite and chlorite are found to be strongly enriched in Li (up to 70 μg/g), Be (up to 8 μg/g) and B (up to 35 μg/g) and with δ^{11}B values of -6 ± 4‰. These new data are consistent with isotopically heavy B being released into the Mariana forearc mantle wedge (serpentinization of dry mantle peridotite after interaction with B-rich slab-released high pH fluids) and confirm models of significant B-loss and B isotope fractionation during forearc (shallow) slab dehydration. The elevated Li, Be and B concentrations in minerals that comprise the bulk of the rocks, namely, amphibole, phengite, and chlorite bear a strong potential to further transport Li and B as well as the isotopically light component of B to greater depths in the mantle, where ongoing metamorphism is responsible for further isotope and elemental fractionation and the formation of distinct mantle reservoirs, e.g. volcanic arc and oceanic intra-plate (OIB) magmas.

1. Introduction

Convergent plate margins are the most dynamic and complex global structures in the Earth's interior. For example at subduction zones input and output 'materials' account for global elemental cycling, where elements are transported from the ocean waters to the sediments and subducted oceanic crust, towards the deep mantle and then back to the surface via arc magmatism. Studies on cross-arc volcanic chains reveal that light element concentrations and isotopic ratios change with increasing depth of the slab and/or distance from the volcanic fronts (or trenches) and that light element contents are always enriched in the metasomatized portion of the mantle (e.g., Chan et al., 1999, 2002; Ishikawa and Nakamura, 1994; Ishikawa and Tera, 1999; Leeman, 1996; Ryan et al., 1995, 1996; Savov et al., 2005b; Tatsumi et al., 1986; Tomascak et al., 2002). Recent light element studies on enriched mantle wedge serpentinites, serpentinite muds, slab-derived pore waters, and metamafic rocks (Bebout et al., 1999; Benton et al., 2001, 2004; Deschamps et al., 2011; Fryer et al., 1999; Kodolányi and Pettke, 2011; Maekawa, 1995; Maekawa et al., 1992,

* Corresponding author at: BHP Billiton Iron Ore, Exploration, PO Box 655, Newman, WA 6753, Australia. Tel.: +61 891268755, +61 487589840(mobile); fax: +61 891448980.
E-mail address: sonja.pabst@gmx.de (S. Pabst).
[1] Present address: Museum Conservation Institute, Smithsonian Institution, Suitland, MD 20746, USA.

0024-4937/$ – see front matter © 2011 Elsevier B.V. All rights reserved.
doi:10.1016/j.lithos.2011.11.010

1993; Mottl et al., 2003; Savov et al., 2004, 2005b, 2007) stress the importance of forearc processes controlling the element recycling within the 'Subduction Factory'.

One of the most complex and lithologically and geochemically diverse region of subduction zones is the slab–mantle interface (décollement) – a region known as a tectonic mélange. Although rarely well preserved, such tectonic mélanges could be exhumed in collision zones and orogenic belts (e.g., Bebout and Barton, 1989; King et al., 2006). Most observations so far were made upon experiments and partially preserved onland exposures, where erosion has exposed ancient subduction-related metamorphic rocks such as those from the Catalina Island in California and Syros Island in Greece (e.g., Bebout, 1995; Bebout et al., 1999; Breeding et al., 2004; Coleman and Clark, 1968; Essene and Fyfe, 1967; King et al., 2006, 2007; Marschall et al., 2006a; Peacock and Hervig, 1999; Sorensen and Grossman, 1989).

In the Izu-Bonin-Mariana convergent margin in the Western Pacific (Fig. 1), the ongoing extrusion of vast amounts of serpentinite muds at large forearc-situated seamounts such as Big Blue, Conical and South Chamorro seamounts (Fryer et al., 2006), emplaces not only serpentinized mantle wedge material, but also a unique suite of metamafic rocks and minerals from depths of up to ~27 km (Fryer et al., 1999, 2000, 2006; Gharib, 2006; Maekawa, 1995; Maekawa et al., 1992, 1993; Savov et al., 2004). The largest volumes of such metamafic clasts are recovered from the South Chamorro Seamount, with Conical, Pacman and Big Blue Seamounts having less of these forearc sourced metamorphic rocks (Fryer et al., 2006; Gharib, 2006; Savov et al., 2004) and no high-pressure minerals were recovered from seamounts closer to the trench (<70 km distance; Gharib, 2006; Maekawa, 1995; Maekawa et al., 1992; Savov et al., 2005a). Up to 8% of the fragments found within the serpentinite mudflows have mafic composition (Fryer, 1992; Fryer and Mottl, 1992; Fryer et al., 1990, 1999, 2006; Gharib et al., 2002; Johnson, 1992; Johnson and Fryer, 1990; Lagabrielle et al., 1992; Maekawa, 1995; Maekawa et al., 1993; Savov et al., 2004, 2005a). Most of these mafic clasts are of blueschist-facies metamorphic grade representing material shed from the downgoing, Jurassic in age, Pacific slab (Fryer et al., 1999; Maekawa, 1995; Maekawa et al., 1993). Due to these recent discoveries, it appears that the Mariana forearc serpentinite seamounts (Figs. 1 and 2) offer an exceptional location for detailed petrological investigation of a great variety of slab-derived material which is the only opportunity to investigate in-situ the workings of an ongoing plate convergence.

Bebout et al. (1993, 1999) examined Li, Be and B whole rock abundances of metasediments and metamafic rocks from the Catalina Schist in California. These rocks exhibit a range of metamorphic grades from lawsonite-albite to greenschist and epidote-amphibolite facies. The high B/Be ratios typically found in both oceanic sediments (B/Be 50–200) and altered oceanic crust (B/Be 5–200; Bebout et al., 1993; Moran et al., 1992; Ryan and Langmuir, 1988, 1993; Spivack et al., 1987) overlap with B/Be ratios in subduction related metamorphic rocks. However, decreasing B concentrations (from ~180 to ~1 μg/g) and decreasing B/Be ratios (from ~140 to ~4) with increasing metamorphic grade in Catalina rocks imply that B, compared to Be, is preferentially removed from the subducting slab during prograde metamorphism and that high B/Be ratios are not retained to subarc depths (Bebout et al., 1993, 1999). Also, B and other highly fluid-mobile elements are initially lost from compacting subducting sediments by devolatilization at shallow depths (Bebout et al., 1993; Kastner and Elderfield, 1993; Kastner et al., 1993; Underwood et al., 2010; You et al., 1993, 1995). Further evidence for light element fractionation and progressive fluid- and fluid mobile element (B, As, Cs, Sb, I) loss from the subducted sediments during subduction is evident by enriched Li, Be and B concentrations in serpentinites of the overlying mantle wedge material,

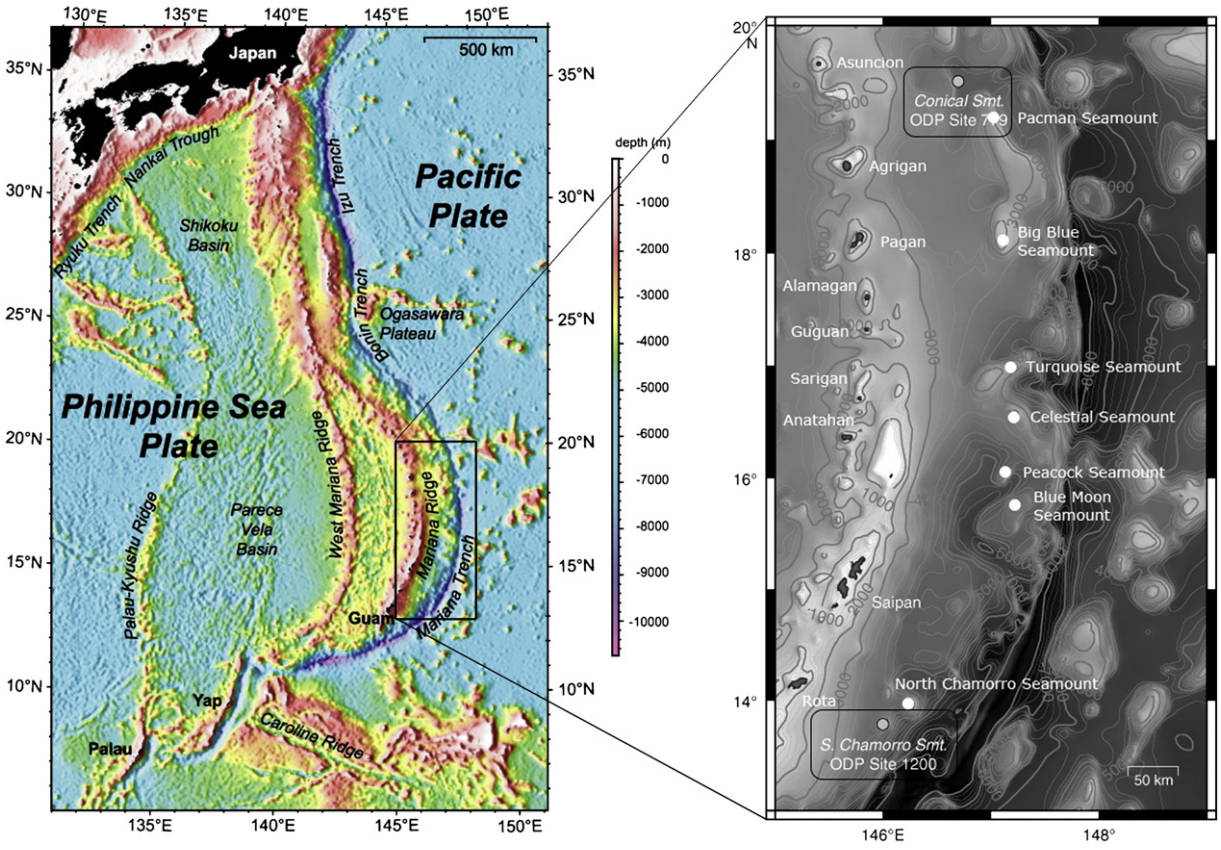

Fig. 1. a) Bathymetry color map of the Izu-Bonin-Mariana arc-basin system (from and after Fryer and Salisbury, 2006), black rectangle indicates the area of figure b), b) Bathymetry map showing volcanic islands and serpentinite mud volcanoes, the seamounts relevant for this study are Conical and South Chamorro Seamount (modified after Snyder et al., 2005).

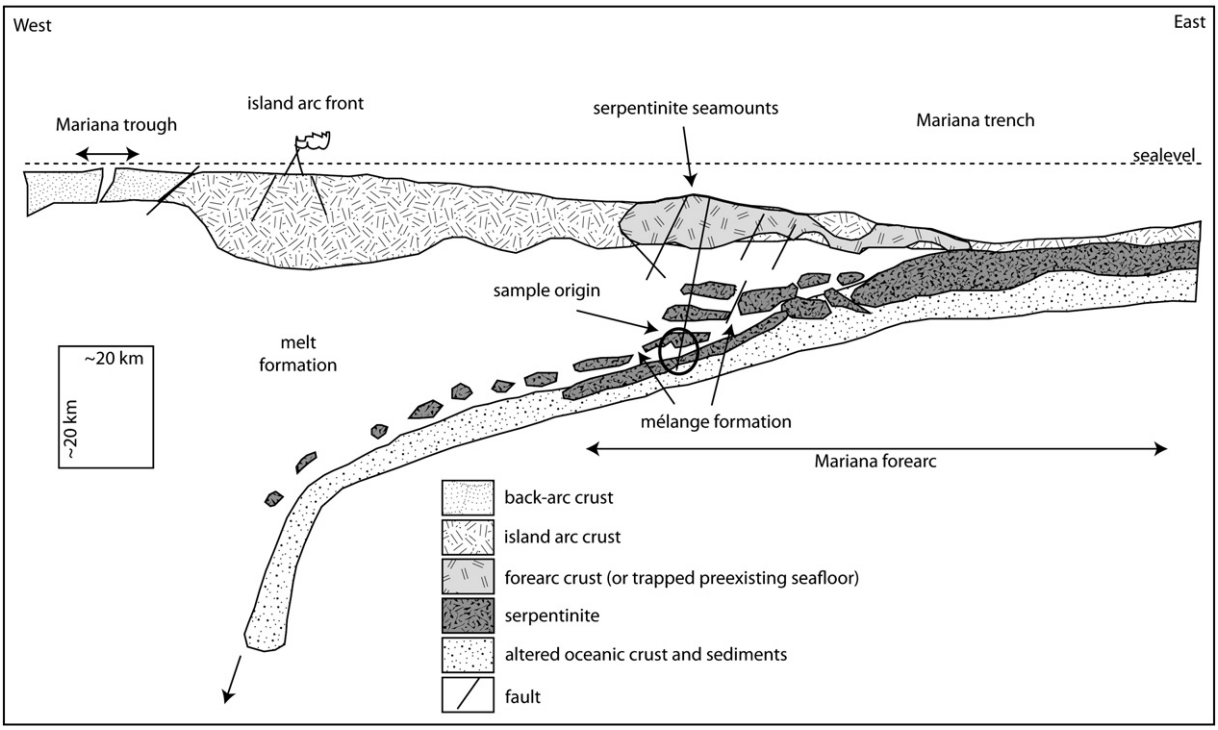

Fig. 2. Cross-section of the non-accretionary Mariana subduction zone in the area of the South Chamorro Seamount, modified after Savov et al. (2007) and adjusted using bathymetric and seismic information from Oakley et al. (2008) and Mottl et al. (1998). The black circle indicates the likely origin of the investigated metamafic rocks.

compositions of extruding forearc fluids and the dramatic across-arc variations of concentrations and isotopic compositions of B, Pb and Li in subduction-related volcanic rocks (Ishikawa and Nakamura, 1994; Ishikawa and Tera, 1997, 1999; Moriguti and Nakamura, 1998; Mottl et al., 2004; Pabst et al., 2011; Ryan and Langmuir, 1987, 1988, 1993; Ryan et al., 1995, 1996; Savov et al., 2009; Tonarini et al., 2001).

B is relatively mobile in aqueous fluids and its redistribution and the fractionation of its isotopic species strongly depends on the thermal evolution and resulting devolatilization history of subducted materials (e.g., Bebout and Nakamura, 2003; Bebout et al., 1993, 1999; King et al., 2007; Marschall et al., 2007; Moran et al., 1992; Nakano and Nakamura, 2001; Peacock and Hervig, 1999). Hence, the preferential loss of the heavier isotope ^{11}B during devolatilization (Leeman and Sisson, 2002; Palmer and Swihart, 1996; Ryan, 2002) decreases $\delta^{11}B$ values of the subducting material with depth. This scenario is supported by several studies on subduction related rocks from onland localities where B contents and B isotopic compositions of metasedimentary rocks appear to be somewhat lower than those of unmodified seafloor sediments (e.g., King et al., 2007; Nakano and Nakamura, 2001; Peacock and Hervig, 1999).

The B isotopic composition of marine sediments (−4 to +3‰, Spivack et al., 1987) and the composition of altered oceanic crust (AOC; +3.4 ± 1.1‰; Smith et al., 1995) differs from subduction related metamorphic rocks with distinctly lower $\delta^{11}B$ values (−3 to −7‰, Peacock and Hervig, 1999. Hence, boron isotope systematics have proven to be important tracers for the characterization of material recycling and metamorphic fluids in subduction zones (Benton et al., 2001; Chaussidon and Jambon, 1994; Chaussidon and Marty, 1995; Ishikawa and Nakamura, 1992, 1993; King et al., 2007; Marschall et al., 2006b; Nakano and Nakamura, 2001; Palmer, 1991; Savov et al., 2004, 2009).

This study presents a detailed petrological and geochemical (Li, Be, B, $\delta^{11}B$) investigation of the metamafic clasts recovered from South Chamorro Seamount (SCS) during ODP Leg 195 (Fryer and Salisbury, 2006; Figs. 1 and 2). It is the first systematic study on the light element inventory of blueschist-facies minerals of actively subducting slabs at an intra-oceanic type convergent margin. Our study provides a high quality dataset uniquely enabling us to see through the complex physical and chemical fluxes occurring at the slab–mantle-interface during the early stages of subduction. Moreover, the ongoing subduction and the increasing P and T with depth forces a further breakdown of specifically these types of hydrous minerals and a release of fluids under arc volcanic fronts. We will explore potential links between forearc dewatering under high pressures that are responsible for blueschist metamorphic assemblage formation, and the impact of such lithologies regarding the efficient recycling of light elements in the subarc mantle.

2. Geological setting and serpentinite mud volcanism of the Mariana forearc

The Izu-Bonin-Mariana (IBM) subduction zone is a non-accretionary intra-oceanic convergent plate margin, which stretches over ~2800 km from near Tokyo (Japan), to south of Guam (Mariana Islands) (Fig. 1). At IBM the Mesozoic Pacific Plate is being subducted west–northwestward beneath the Philippine Sea plate (Stern et al., 2003; Uyeda, 1982; Uyeda and Kanamori, 1979).

The region developed since the Early-Middle Eocene (48 Ma ago) with the onset of westward subsidence of old, dense Jurassic–Cretaceous Pacific crust beneath the Philippine Sea plate (Bloomer et al., 1995; Cosca et al., 1998; Seno and Maruyama, 1984; Stern and Bloomer, 1992). Currently, in the Mariana segment of the convergent margin, the Pacific plate descends at a 20° dip angle to ~60 km depths, while at depths >100 km it sinks almost vertically beneath the Philippine Sea plate (Engdahl et al., 1998; Fryer et al., 1990). Converging rates of the Pacific plate were modeled by Seno et al. (1993) and reach ~20 mm/yr moving in NW direction at 12°N and ~60 mm/yr moving WNW at 34°N. In consequence, plate motions under Conical and South Chamorro seamounts equal to ~43 mm/yr and ~23 mm/yr, respectively.

Seismic investigations of the southern Mariana subduction zone suggest a depth to the slab of >25 km below sea level, i.e., >22 km below seafloor (kmbsf) at ~85 km distance from the trench (below South Chamorro Seamount; e.g., Oakley et al., 2008). Numerous 2–3 km high seamounts have been well documented on the Pacific plate entering the Marianas Trench (Fryer and Fryer, 1987; Fryer and Smoot, 1985). Nevertheless, there seems to be no conclusive geophysical evidence for significant tectonic deformation of the Mariana forearc crust due to collision with such seamounts (Oakley et al., 2008). Despite that, the Mariana forearc between the trench and the arc is pervasively faulted by tectonic activity (Horine et al., 1990; Salisbury et al., 2002). Within deep reaching faults of the forearc, serpentinite gouges mix with rising slab-derived fluids. This mud-rock-mixture buoyantly rises until it ultimately extrudes on the seafloor to form numerous km-scale seamounts, i.e., serpentinite mud volcanoes (e.g., Fryer, 1992; Fryer et al., 2006; Hussong and Fryer, 1982). They are located on the outer forearc of the Mariana margin in a trench-parallel zone ~30 to 100 km arcwards of the trench axis (between trench and arc) and can reach up to 40 km in diameter and over 2 km in height (Fryer, 1992; Fryer et al., 2000, 2006). Unconsolidated flows of clay- to silt-sized serpentinite mud enclose up to boulder-sized clasts of variably serpentinized mantle peridotite and subordinately blueschist-facies clasts (Fryer and Hussong, 1982; Fryer and Todd, 1999; Fryer et al., 1990, 2000, 2006; Gharib, 2006; Maekawa, 1995; Maekawa et al., 1992; Salisbury et al., 2002; Savov et al., 2004) that permit the direct sampling of slab-derived material (see Fig. 2).

3. Sample selection and analytical techniques

Samples were selected from drill cores recovered at the SCS during ODP Leg 195, at Site 1200 during cruises of the Drilling Vessel JOIDES Resolution (Salisbury et al., 2002). The SCS is located at a water depth of 2930 m below seafloor (mbsf) at 13°47′ N, 146°00′ E, ~125 km east of Guam Island and 85 km west of the trench (Figs. 1 and 2). Unconsolidated serpentinite mud was recovered as whole-round sections of cores from piston drilling and then ~10 cm intervals were squeezed to mud-pellets for pore fluid extractions (e.g., Salisbury et al., 2002). A total of eleven mud-pellets (representing more than one meter of drill section) were dissolved in distilled water and fragments of interest were hand-picked quantitatively and then sorted using a Leica WILD M10 binocular microscope. This procedure was necessary due to the weak texture of most fragments and their overall small size varying from <1 mm to several mm. A total of about 50 metamafic clasts was prepared as 1-inch round polished sections (not impregnated) appropriate for the secondary ion mass spectrometer (SIMS) at the Institut für Geowissenschaften, Universität Heidelberg, Germany. The high number of fragments of our study considerably increases the amount and knowledge extracted from previously studied metamafic samples from the Mariana forearc (e.g., Fryer, 1992; Fryer et al., 2006; Gharib et al., 2002; Johnson, 1992; Maekawa, 1995; Maekawa et al., 1993; Savov et al., 2005a). In Table 1 we list the studied intervals from SCS containing metamafic rock clasts (e.g., chlorite-amphibole-schists).

Major element compositions of mineral phases were determined using a Cameca SX 51 electron microprobe (EPMA) equipped with five wavelength-dispersive spectrometers (Institut für Geowissenschaften, Universität Heidelberg, Germany). Operating conditions were 20 nA beam current and 15 kV acceleration voltage. Spot size was 1 μm with counting times of generally 10 s for peak and 5 s for background for all elements. Synthetic and natural oxides and silicates were used as reference materials. Examination by EPMA and SIMS required detailed petrographic documentation of the samples (e.g., textures and mineral relationships) for choosing appropriate targets for further analysis; sections were investigated by polarizing microscopy followed by back-scattered electron (BSE) imaging using a high resolution LEO 440 scanning electron microscope (SEM) coupled with energy-dispersive X-ray spectrometer (EDS) at the Institut für Geowissenschaften, Universität Heidelberg, Germany. The applied accelerating voltage was 15 kV and probe current was ~2–5 nA. Carbon-coated polished sections were used for both BSE investigation and electron microprobe analyses.

Li, Be and B were analyzed in-situ on polished sections by Secondary Ion Mass Spectrometry (SIMS) using a modified Cameca ims 3f ion microprobe at the Institut für Geowissenschaften, Universität Heidelberg, Germany. Analyses were performed using a 14.5 keV/20 nA $^{16}O^-$ primary beam and acceleration to a nominal energy of 4.5 keV for the positive secondary ions. Secondary ^{7}Li, ^{9}Be, ^{11}B and ^{30}Si ions were collected with the energy window set to 40 eV and applying the energy filtering method using an offset of 75 eV at a mass resolution ($m/\Delta m$) of about 1040 to suppress interfering molecules and to minimize matrix effects (Ottolini et al., 1993). Secondary ion intensities were normalized to the count rates of ^{30}Si and calibrated against the NIST SRM610 glass reference material using the concentrations (preferred averages) from Pearce et al. (1997). The accuracy is estimated to be <20% for Li and <10% for Be and B for concentrations in excess of 0.1 μg/g (Ottolini et al., 1993). Element concentrations were quantified using the Si values of the corresponding EPMA analysis. Each analysis comprised 10 cycles for each isotope with integration times of 4 s/cycle for Li and Be, 8 s/cycle for B, and 2 s/cycle for Si. The setup chosen and the background of 0.02 ions/s ('well known background') lead to a detection limit (critical value) of 1.9 ng/g (Li), 1.8 ng/g (Be), and 6.9 ng/g (B) (Currie, 1968; Marschall and Ludwig, 2004). Due to these low blank levels, the results were not background corrected. We used the standard procedure of Marschall and Ludwig (2004) in order to reduce possible surface contamination during polished section preparation. Applying field apertures suppress contaminating secondary ions from the crater edges (Benninghoven et al., 1987) and set the imaged field smaller than the primary beam diameter and enables analyses of <6 μm spot size.

Boron isotopic composition was determined using a VG Isomass 54E positive thermal ionization mass spectrometer, following

Table 1
Summary of intervals containing metamafic material of holes 1200D, E, and F, South Chamorro Seamount, ODP Leg 195.

ODP Leg	Hole	Core	Section	Interval	Depth in mbsf[a]	Label	Sample type	Serpentinite	Metabasics
195	1200D	001H	04WR	130–140	5.80	D1H4	Mud-pellet	x	x
195	1200D	003H	01WR	130–140	11.20	D3H1	Mud-pellet	x	x
195	1200E	001H	03WR	130–140	4.30	E1H3	Mud-pellet	x	x
195	1200E	002H	02WR	130–140	8.90	E2H2	Mud-pellet	x	x
195	1200E	004H	01WR	130–140	13.30	E4H1	Mud-pellet	x	x
195	1200E	004H	02WR	130–140	14.80	E4H2	Mud-pellet	x	x
195	1200E	007H	02WR	130–140	28.70	E7H2	Mud-pellet	x	x
195	1200F	001H	01WR	90–105	0.90	F1H1	Mud-pellet	x	x
195	1200F	001H	03WR	140–150	4.40	F1H3	Mud-pellet	x	x
195	1200F	001H	04WR	140–150	5.90	F1H4	Mud-pellet	x	x
195	1200F	002H	02WR	140–150	10.60	F2H2	Mud-pellet	x	x

[a] Data from http://iodp.tamu.edu/janusweb/coring_summaries/.

separation of boron by ion-exchange procedures as described by Tonarini et al. (2003). Total procedural blanks (30–40 ng) are negligible relative to the amount of sample processed (about 2000 ng). Isotopic fractionation associated with mass spectrometric analysis was eliminated using a fractionation factor, calculated as $\{R_{cert} + 0.00079/R_{meas}\}$, relative to NIST SRM 951 ($^{11}B/^{10}B_{meas} = 4.0498 \pm 0.0010$) which was processed identically with each batch of samples. Boron isotopic composition is reported in conventional delta notation ($\delta^{11}B$) as per mil (‰) deviation from the accepted composition of NIST SRM −951 (certified $^{11}B/^{10}B = 4.04362$; Catanzaro et al., 1970). Precision and accuracy of isotopically homogeneous samples treated with alkaline fusion chemistry are estimated conservatively as ±0.5‰ (Tonarini et al., 2003) based on replicate determinations for samples and for repeated analyses for standard rock JB-2 ($\delta^{11}B = 7.25 \pm 0.32$‰ ($2\sigma$), $n = 33$ analyses with independent chemistry).

Boron isotope ratios were determined on B-rich minerals using the Cameca ims 3f ion microprobe at the Institut für Geowissenschaften, Universität Heidelberg, Germany. Primary ion beam was $^{16}O^-$ accelerated to 10 keV with a beam current of 10–20 nA. The diameter of the 10 nA spot was <20 μm and increased to ~40 μm with 20 nA beam current. The energy window was set to 100 eV without offset to the secondary accelerating voltage. Mass resolution (m/Δm) was ~1175. On each analysis spot 400 cycles were measured (only 200 for analyses E1H3-A1,2 and E1H3-4D2,4,5) with counting times of 2×1.66 s and 1.66 s on ^{10}B and ^{11}B, respectively. The B6 obsidian (Tonarini et al., 2003) was used as reference material for the in-situ B isotope analyses with SIMS. Reproducibility for standard analyses was ~0.5‰ (1σ).

SIMS analyses of $\delta^{11}B$ are dependent on the matrix of the sample material and $\delta^{11}B$ values often differ from $\delta^{11}B$ measured via TIMS techniques (e.g., Rosner et al., 2008). With the same SIMS instrument in Heidelberg, B isotopes have been successfully analyzed for tourmaline and phengite (Marschall, 2005). The results were cross-calibrated, i.e. matrix-matched with the same sample material analyzed by TIMS (Altherr et al., 2004; Marschall et al., 2006b). For this study, the minerals amphibole '21805' and phengite 'Phe-80-3', which are chemically homogeneous crystals, have been analyzed by SIMS and by TIMS. Using the obsidian B6 (Tonarini et al., 2003) as a primary reference material, SIMS $\delta^{11}B$ values are -3.1 ± 1.9‰ (1σ, $N = 15$) for amphibole '21805' and -14.8 ± 2.8‰ (1σ, $N = 10$) for phengite 'Phe-80-3', while the TIMS $\delta^{11}B$ values are -0.37 ± 0.44‰ (1σ, $N = 2$) for amphibole and -13.50 ± 0.35‰ (1σ, $N = 2$) for phengite. Due to the offset between SIMS and TIMS values of 2.8‰ for amphibole and 1.3‰ for phengite (Fig. 3; Table 2) we use these crystals as primary standards in our study and apply a conservative correction value of 3‰ for amphibole and phengite analyses. B isotope data for chlorite crystals were corrected with the use of these same crystals as there is lack of chlorite reference materials with sufficiently high B concentrations.

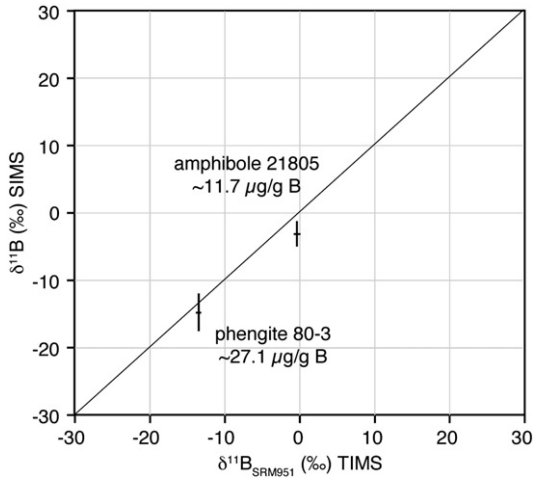

Fig. 3. Comparison of boron isotope ratios analyzed by TIMS and SIMS for amphibole '21805' and phengite 'Phe-80-3'. Symbol line lengths have 1σ error size. For values see Table 3.

Table 2
Comparison of B isotope analyses by SIMS and TIMS.

	Am '21805'	Phe '80-3'
SIMS		
Mean Li content (μg/g)	0.09	32.09
1σ	0.02	4.5
Mean B content (μg/g)	11.69	27.13
1σ	1.2	1.3
Mean $\delta^{11}B$ (‰)	−3.12	−14.76
1σ	1.9	2.8
N	15	10
TIMS		
$\delta^{11}B$ (‰)	−0.37	−13.50
1σ	0.44	0.35
N	2	2
Deviation SIMS-TIMS	−2.75	−1.26

SIMS analyses were performed with 10–25 nA beam current and calibrated against B6 obsidian.

Element distribution maps were obtained using an ION-TOF GmbH ToF-SIMS IV instrument at Smithsonian Institution's National Museum of Natural History in Washington D.C., USA. ToF-SIMS is a surface-sensitive method that uses a pulsed primary ion beam (e.g., Ga^+, Bi^+, Cs^+ or O_2^+) to sputter atoms and molecules from the topmost atomic monolayers of the surface. The fraction of the secondary particles that are ionized during this process (~1%) is then electrostatically accelerated into a 'flight tube' (field-free drift region), where the ions separate according to their velocities that depend on their masses. Thus, their masses are determined by measuring the exact time at which they reach the detector (i.e., time-of-flight), resulting in a secondary ion mass spectrum. While rastering the finely focused beam over the sample surface, all secondary ion arrival times are recorded together with the information of their spatial origin. For this study, a 25 kV $^{69}Ga^+$ primary ion column was operated in single crossover mode with a cycle time of 50 μs, allowing for optimum lateral resolution of ~300 nm. To remove surface contamination, the mapping area was sputter-cleaned with a 3 keV Ar^+ ion beam. For silicates, the sensitivity for the detection of Li^+ is about 17 times higher than for B^+ (Stephan, 2001). Also, the sensitivity of Li and B changes between minerals, i.e., identical Li contents can result in different count-rates.

4. Results

4.1. Petrography

The metamafic rock fragments recovered from SCS comprise a great variety of mineral assemblages and are all generally <5 mm in diameter. There are some samples where non-foliated textures were observed, but commonly these rocks exhibit schistosity defined by oriented crystals of chlorite, phengite and/or amphibole. Although finely comminuted by the drilling and squeezing of the serpentinite mud, the clasts still preserve important textural and petrological information. The rocks were extracted from different depths and drill core locations on the SCS summit area (Table 1) and therefore we consider them as representative for the material carried in the mud flows. Accordingly, about 50 clasts from eleven individual core sections were separated and thoroughly investigated. Clasts that show the same mineral content and textures and that were recovered from the same mud-pellet are considered as representing one rock piece. The studied clasts reveal a great variety of mineral assemblages, however, fragments can generally be divided into amphibole-(talc-)chlorite-schists, chlorite-epidote-schists and amphibole-chlorite-phengite-

schists (Table 3). In addition, few samples show almost monomineralic aggregates (talc, amphibole). Due to the very small clast sizes, it is often impossible to determine if these are parts of larger rock pieces or metasomatic products.

Other fragments are rocks with magmatic protolith (samples F2H2-5c + d, E7H2-10f, E1H3-3 d) and exotic schists composed of andradite garnet in a fine-grained serpentine (antigorite) matrix (samples E2H2-4 g + 5 h) or 'hydrous Cr-garnet' grains with picotite cores embedded in a fine grained serpentine matrix (sample E4H2-2a) or tiny andradite grains that are concentrated in chlorite layers that are foliated and intergrown with biotite and accessory spinel (sample D3H1-8c; Fig. 4a). Some of these samples might represent fragments of volcanic arc erosion or entrained oceanic crust material (under the seamount) sampled by the rising serpentinite muds. However, this study aims to discuss light element concentrations and boron isotope values of blueschist-facies rocks of broadly mafic composition (i.e., the subducting slab material). Hence, these latter rock types will not be discussed further. Detailed information about these rocks can be found in Pabst (2009).

4.1.1. Amphibole-talc-chlorite-schists

This is the most common rock variety recovered from SCS and is dominated by the paragenesis amphibole + chlorite + talc of varying abundance. Apatite, spinel, titanite, zircon, pyroxene, rutile and magnetite are present in some samples. Rock fragments include:

1) amphibole-free talc-schists with minor chromian magnetite (Fig. 4b);
2) magnetite-bearing fine-grained and foliated tremolite schists with talc and chlorite (more talc for less chlorite and vice-versa);
3) apatite-bearing amphibole-chlorite-talc-schist. The amphiboles are actinolite, magnesio-hornblende and winchite;
4) amphibole-chlorite-talc-schist with patchy zoned amphiboles. The amphiboles are actinolite-tremolite, magnesio-riebeckite to winchite and magnesio-cummingtonite;
5) amphibole (tremolite)-chlorite-talc-schist with apatite, titanite, ilmenite and zircon;
6) chlorite-amphibole-schists with no accessory minerals. Amphiboles are tremolite or actinolite with either tremolite or edenite cores (Fig. 4c);
7) strongly foliated and strongly folded fine-grained amphibole-chlorite-schist with apatite- and titanite-enriched bands and patchy zoned amphiboles of tremolite-actinolite and magnesio-hornblende-edenite composition;
8) coarse-grained weakly foliated chlorite-amphibole (actinolite)-schists with titanite, apatite and zircon;
9) monomineralic tremolite-actinolite-aggregates (e.g., hornblendite), and
10) chlorite-amphibole-schists with varying amounts of accessory apatite, titanite, pyroxene and rutile. Amphiboles lack zonation and are magnesio-hornblende and actinolite in composition, while the pyroxenes are augite-diopside ($En_{41}Fs_{13}Wo_{46}$.).

More massive rock types are chlorite-aggregates with accessory titanite and chlorite-amphibole-aggregates with accessory magnetite. Amphibole compositions are Mg-hornblende, actinolite and edenite.

4.1.2. Chlorite-epidote-schists

The chlorite-epidote-schists are characterized by epidote porphyroblasts and (Na-rich) amphiboles and a large variety of accessory

Table 3
Estimated modal composition (vol.%) of blueschist-facies clasts ODP Leg 195, South Chamorro Seamount.

Sample	Depth (mbsf)	Rock type	srp	tlc	chl	am	phe	ep	aln	ap	ttn	spl	px	pmp	rt	zrc	grt	Others
D1H4	5.85	chlorite-aggregate	–	–	82	–	–	–	–	–	18	–	–	–	–	–	–	–
D1H4-1a	5.85	am-chl-schist	–	5	32	63	–	–	–	–	–	–	–	–	–	–	–	–
D1H4-2d	5.85	am-chl-schist	–	–	59	33	–	–	–	2	6	–	–	–	–	<1	–	–
D3H1-8C	11.25	chl-bt-schist	–	–	55	–	–	–	–	–	–	<1	–	–	–	–	3	42 bt
E1H3-3d	4.35	chl-am-rock	–	–	90	8	–	–	–	2	–	–	–	–	–	–	–	–
E1H3-4a	4.35	phe-chl-am-schist	–	–	38	16	37	<1	–	4	2	3	–	–	<1	–	–	–
E1H3-4b	4.35	chl-am-ep-rock	–	–	27	62	<1	4	<1	–	2	<1	<1	<1	4	<1	–	–
E1H3-4c	4.35	chl-ep-grt-rock	–	–	50	4	–	25	<1	10	3	2	–	–	<1	<1	6	–
E1H3-4d	4.35	phe-am-chl-schist	–	–	25	42	30	–	–	–	3	–	–	–	–	–	–	–
E1H3-5, 2x	4.35	am-chl-schist	–	–	70	30	–	–	–	–	–	–	–	–	–	–	–	–
E2H2-4b	8.95	chl-am-ap-rock	–	–	51(d) + 27(l)	10	–	–	–	1	1	–	10	–	–	–	–	–
E2H2-4j	8.95	amphibole-aggregate	–	–	–	100	–	–	–	–	–	–	–	–	–	–	–	–
E2H2-5d	8.95	am-chl-tlc-rock	–	28	28	42	–	–	–	2	–	–	–	–	–	–	–	–
E2H2-5j	8.95	talc-aggregate	–	92	–	–	–	–	–	–	–	2	–	–	–	–	–	6
E4H1-2a	13.35	chlorite-amphibole	–	–	58	42	–	–	–	–	–	<1	–	–	–	–	–	–
E4H2-2b	14.85	chl-ep-rock	–	–	38	–	–	58	–	2	2	–	–	–	–	–	–	–
E7H2-1a,b,2a,8a,b,10	28.75	am-chl-schist	–	–	28	68	–	–	–	2	2	–	–	–	–	–	–	–
E7H2-6A	28.75	chlorite-aggregate	–	–	63(d) + 34(l)	–	–	–	–	–	3	–	–	–	–	–	–	–
F1H1-3C	0.98	am-chl-schist	–	–	50	50	–	–	–	–	–	–	–	–	–	–	–	–
F1H1-3D	0.98	chl(-phe)-schist	–	–	97	–	3	–	–	–	–	<1	–	–	–	–	–	–
F1H1-3E	0.98	am-chl-rock	–	–	42	45	–	–	–	4	4	–	5	–	<1	–	–	–
F1H1-3F	0.98	am-chl-schist	–	–	50	50	–	–	–	–	–	–	–	–	–	–	–	–
F1H3-2C	4.45	chl-tlc-am-schist	–	76	8	16	–	–	–	–	–	<1	–	–	–	–	–	–
F1H3-2D	4.45	chlorite-aggregate	–	–	91	–	–	–	–	–	9	–	–	–	–	–	–	–
F1H3-2F	4.45	am-(tlc)-rock	–	60	–	40	–	–	–	–	–	–	–	–	–	–	–	–
F1H4-3a	5.95	chl-ep-rock	–	–	67	–	–	30	in ep	–	3	<1	–	–	–	–	–	<1
F1H4-5	5.95	am-chl-schist	–	–	55	45	–	–	–	–	–	–	–	–	–	–	–	–
F2H2-1A	10.65	am-chl-ep-schist	–	–	26	30	–	22	1	20	1	–	–	–	–	<1	–	<1
F2H2-3F	10.65	amphibole-aggregate	–	–	–	100	–	–	–	–	–	–	–	–	–	–	–	–
F2H2-4A,B,H	10.65	phe-am-chl-schist	–	–	8	47	39	–	–	<1	3	–	3	–	–	<1	–	–
F2H2-4D	10.65	chl-am-schist	–	–	30	65	–	–	–	<1	<1	–	5	–	–	–	–	–
F2H2-4E,G, 5G	10.65	chl(−am)-schist	–	7	69	22.5	–	–	–	<1	<1	1	–	–	–	<1	–	–
F2H2-4F,J	10.65	chl(-am)-schist	–	5	85	10	–	–	–	–	–	–	–	–	–	–	–	–
F2H2-5A	10.65	phe-am-schist	–	–	13	59	23	–	–	<1	3	–	2	–	<1	<1	–	–

Visual mineral volume% estimation. d = dark. l = light.
Mineral abbreviations – srp: serpentine. tlc: talc. chl: chlorite. am: amphibole. phe: phengite. ep: epidote. aln: allanite. ap: apatite. ttn: titanite. spl: spinel. px: (Na-)pyroxene. pmp: pumpellyite. rt: rutile. zrc: zircon. grt: garnet. bt: biotite.

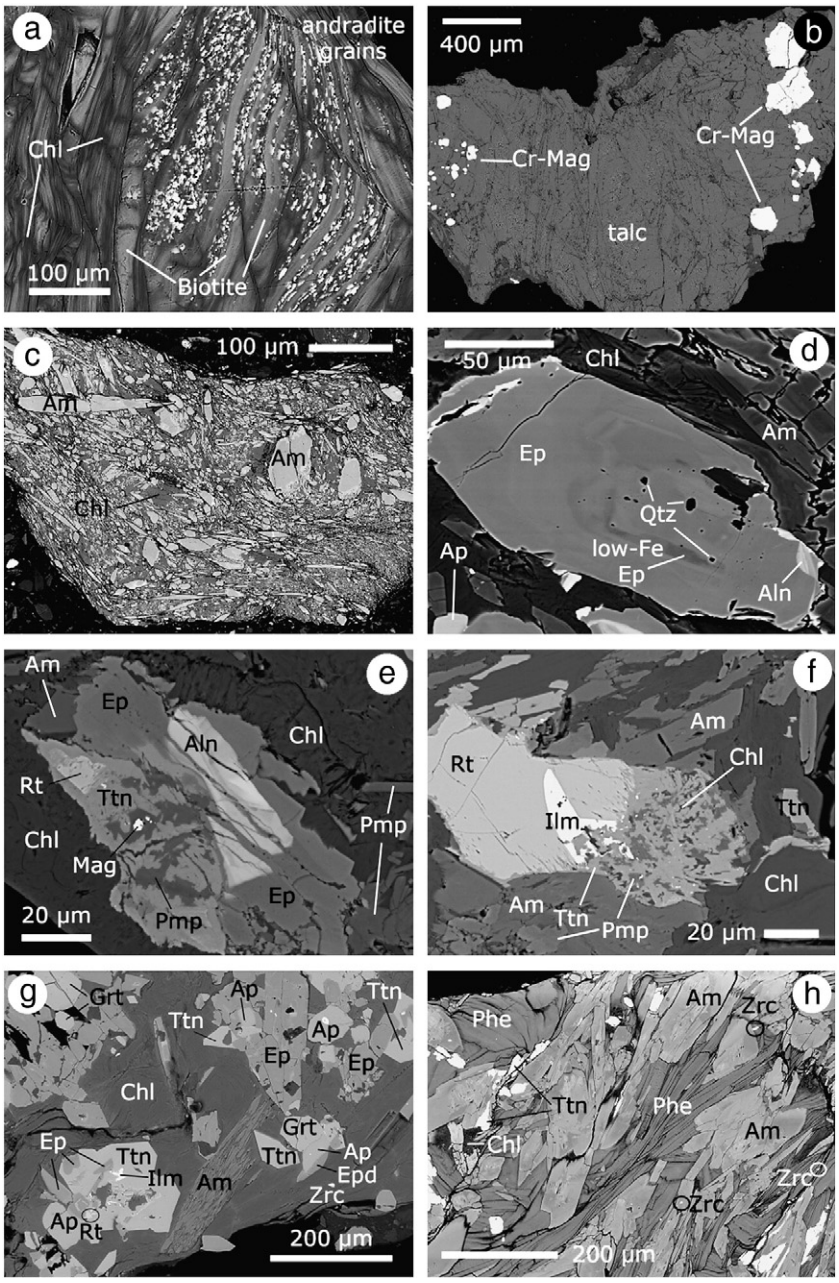

Fig. 4. Back-scattered electron (BSE) images of a) biotite-chlorite schist with garnet and accessory spinel, b) talc-schist, c) fine-grained amphibole-chlorite-schist, d) zoned epidote with quartz-inclusions in a chlorite-amphibole-schist, e + f) pumpellyite-epidote-(Na-)amphibole-assemblage in a amphibole-chlorite-schist, g) garnet- and epidote-bearing rock fragment, h) phengite-rich amphibole-chlorite schist. Mineral abbreviations after Kretz (1983): Aln = allanite, Ap = apatite, Am = amphibole, Chl = chlorite, Ep = epidote, Grt = garnet, Ilm = ilmenite, Mag = magnetite, Phe = phengite, Pmp = pumpellyite, Qtz = quartz, Rt = rutile, Ttn = titanite, Zrc = zircon.

phases such as ilmenite, titanite, apatite and garnet enclosed in a chlorite matrix. Apatite, titanite, allanite, zircon and ilmenite are common trace minerals, whereas magnetite is relatively rare. The following chlorite-epidote-schist types can be distinguished:

1) One albite-bearing sample (F1H4-3a) is dominated by chlorite + epidote (Xps = 0.33) + titanite. Magnetite and albite occur as µm scale rounded inclusions in epidote, patchy titanite was found as inclusions in or overgrowths with epidote and partly surrounds allanite.
2) One quartz-bearing sample (Fig. 4d; F2H2-1a) is composed of coarse-grained amphibole, epidote (with trace amounts of allanite) and apatite embedded in a matrix of platy chlorite. Amphibole crystals are elongated and often irregularly zoned, some have patchy cores. Compositions vary from Mg-hornblende in the cores to glaucophane in the rims. Also zonations between actinolite-winchite can be observed. Other amphibole crystals have edenite cores surrounded by actinolite-winchite zonations. Aside from amphibole-rich areas, there are epidote-apatite-titanite rich areas in the sample. Besides traces of titanite, further minerals are zircon and inclusions of α-quartz in epidote (confirmed by Raman spectroscopy). Apatite and titanite also occur as single grain inclusions in amphibole.
3) Fig. 4e + f show a sample dominated by an amphibole-chlorite matrix with minor epidote, allanite, rutile, titanite and traces of ilmenite, phengite, pyroxene, pumpellyite, zircon and magnetite (E1H3-4b). The sample also hosts rare actinolite, pargasite/Mg-hastingite and more frequently edenite amphibole, crystallized as predominantly zoned, subhedral grains. Patchy amphibole with Na-rich spots has Mg-hornblende composition. Rims of

amphibole needles and some internal bands have Na-rich (winchite and richterite) composition. Amphiboles enclose rutile, ilmenite and epidote grains. Rutile and ilmenite always occur together (ilmenite as an exsolution from rutile) and they partly reacted to form (i) titanite, which surrounds the rutile, or (ii) larger titanite grains, which include patches of pumpellyite and sometimes chlorite. The pumpellyite can also contain small magnetite grains. The reaction Rt + Ilm → Ttn + Pmp + Mag requires addition of Ca, which most likely is sourced from the surrounding amphiboles. Epidote has allanite cores and inclusions of rutile-zircon aggregates. Zircon may also be found as single grains within amphibole. The epidote-allanite assemblages occur in contact with the rutile-titanite-pumpellyite-magnetite assemblages. Pyroxene is in assemblage with amphibole and chlorite as euhedral crystals and has variable aegirine-augite composition (7–26 mol% Jd). Tiny phengite needles are aligned to amphibole near epidote rich assemblages.

4) In one garnet-bearing sample (E1H3-4c) the dominant phase is platy matrix chlorite embedding irregularly distributed epidote (with allanite rich zones), minor apatite, garnet, amphibole, titanite, spinel and trace amounts of rutile, zircon and allanite. Garnet occurs as single euhedral grains, often surrounded by epidote, titanite and chlorite, while it seems to replace epidote (Fig. 4g). Apatite is sub- to euhedral and occurs together with epidote, but is also found as inclusions in epidote and as tiny round inclusions in the centre of garnets. The average garnet composition is $Prp_{12}Alm_{22}Sps_{48}Grs_{11}Adr_{7}$. Cracks in the epidote and garnet grains are filled with chlorite. Zircon grains are found as inclusion in chlorite, apatite and epidote. Rutile and ilmenite inclusions are found in titanite, which on the other hand includes patches of epidote. Amphibole occurs as aggregates of small anhedral needles of winchite composition.

Another sample is an epidote-apatite-titanite aggregate (E4H2-2b) which is composed of variably sized epidote grains distributed in a chlorite matrix. Apatite grains occur together with the epidote and titanite and accumulate in some areas of the sample.

4.1.3. Amphibole-chlorite-phengite-schists

Amphibole-chlorite-phengite-schists are characterized by variable amounts of amphibole, chlorite and phengite as major constituents.

1) Coarse-grained schists have a foliation defined by elongated amphibole needles and phengite sheaves in a chlorite matrix (Fig. 4h). Amphiboles have irregular to patchy zonation with compositions between actinolite, magnesio-hornblende and magnesio-riebeckite (F2H2-5a) and actinolite with rare Mg-hornblende in core-like areas, Mg-riebeckite in rim-like areas, and winchite in thin fissure-like veins within amphibole (F2H2-4a,b,h). Interstitial elongated pyroxene aggregates have aegirine composition with up to 28% jadeite component (F2H2-5a) and ~19% Jd component (F2H2-4a,b,h), respectively. Titanite occurs as interstitial irregular formed grains. Trace minerals are rutile as inclusions in titanite and amphibole, apatite as inclusions in amphibole, solely tiny zircon grains and zircon and apatite as inclusions in titanite.
2) In fine-grained schist (E1H3-4a) phengite sheaves and unzoned amphiboles (winchite to Mg-riebeckite composition) in a chlorite matrix define the foliation. Large apatite grains occur in minor amounts, irregularly shaped ilmenite occurs in assemblages with titanite and epidote. Rutile, epidote and titano-magnetite occur as inclusions in ilmenite, epidote also in apatite.
3) In phengite-schist, dominated by large (~1 mm long) oriented and well-crystallized phengite sheaves, amphibole with Mg-hornblende composition and titanite are intergrown in a chlorite matrix (E1H3-4d).
4) In chlorite-dominated schists (F1H1-3 d), small phengite sheaves are irregularly distributed with little spinel.

4.1.4. Modal major-element composition of metamafic rocks

To estimate the volume fraction of the minerals, gray-scale backscattered images were evaluated using the visualizing software ImageJ 1.39 t (National Institutes of Health, USA). Modal abundances of mineral assemblages in the recovered mafic clasts are reported in Table 3. Although the size of the rock fragments is very small, the volume % estimations are statistically representative due to the very small mineral grain size within the fragments.

Combining the modal abundance (Table 3) and compositions of relevant mineral phases (see electronic appendix A1) gives the bulk rock composition of the mafic samples (Table 5). The FeO content of minerals was recalculated to Fe_2O_3. It should be stressed that our South Chamorro bulk rock compositions bear errors owing to the visual mineral volume % estimation and the averaging of variable mineral compositions (e.g., amphibole) of the very small metamafic clasts. Amongst the 50 clasts, seven clasts are large (>6 mm) and show about 600 to 20,000 grains available for counting. Statistically, this means that for these seven clasts, major phases (modal abundance >10%) can be estimated with better than 15%. Further, we have to keep in mind that the studied clasts are pieces of larger fragments that broke apart along weak zones within the rock and that therefore, weaker minerals from such fracture zones were preferentially incorporated into the surrounding serpentine-mud matrix.

The metamafic rocks show a wide range in their SiO_2 (31–65 wt.%) and Al_2O_3 (up to 23 wt.%) abundances (Fig. 5; Table 5). Talc- and/or amphibole-rich samples have the highest SiO_2 contents, whereas chlorite- and epidote-rich samples are relatively silica-poor. To the contrary, Al_2O_3 concentrations increase from talc- and amphibole-rich samples to chlorite- and epidote-rich samples. The estimated Mg# ranges from 39 to 92 and the average H_2O-content is ~8 wt.%. The mean composition of all samples is ~46 wt.% SiO_2, ~24 wt.% MgO and ~0.8 wt.% TiO_2 with low total alkali (Na + K) content (<7 wt.%). A similar major element composition is reported for Conical and Big Blue Seamounts metamafic rocks (Gharib, 2006), metabasalt and metadiabase fragments from Conical and South Chamorro Seamounts (Johnson, 1992; Savov et al., 2005a) as well as basalts from Sites 801 and 1149 outboard of the IBM margin (Kelley et al., 2003) and altered basalts from the Mid-Atlantic Ridge (seawater-altered basalts from ODP Hole 504B; Alt et al., 1986; Mottl, 1983). It has been suggested that Mariana forearc metamafic rocks have a variously modified mid-ocean-ridge basalt (MORB-like) protolith (Gharib, 2006; Savov et al., 2005a). Nevertheless, our study considerably increases the data collection on Mariana slab and slab–mantle-interface rocks by displaying tremendous variations in their mineral assemblages and a significantly broader range of bulk rock compositions of South Chamorro metamafic rocks (Table 5) compared to previous studies.

4.2. Light element concentrations

4.2.1. ToF-SIMS

The Li and B distribution in selected fragments was mapped by ToF-SIMS in order to assess the element distribution between phases. Fig. 6a + b shows Li and B distribution maps of fragment E1H3-4d. The highest Li content (i.e., count-rates) was recorded in chlorite and phengite, with significantly less Li residing in amphibole. Chlorite and amphibole show low B contents relative to phengite, which is enriched in B.

Fig. 6c + d shows ToF-SIMS Li and B distribution maps of sample E1H3-4B. Similarly to the previous sample, Li shows very high concentrations in chlorite and phengite and is much less abundant in the amphiboles. Phengite shows the highest B contents, whereas chlorite shows highly variable B concentrations. Amphibole and other mineral phases mainly lack B.

Overall the ToF-SIMS elemental mapping reveals that phengite, chlorite and amphibole are the major Li carriers in these rocks and

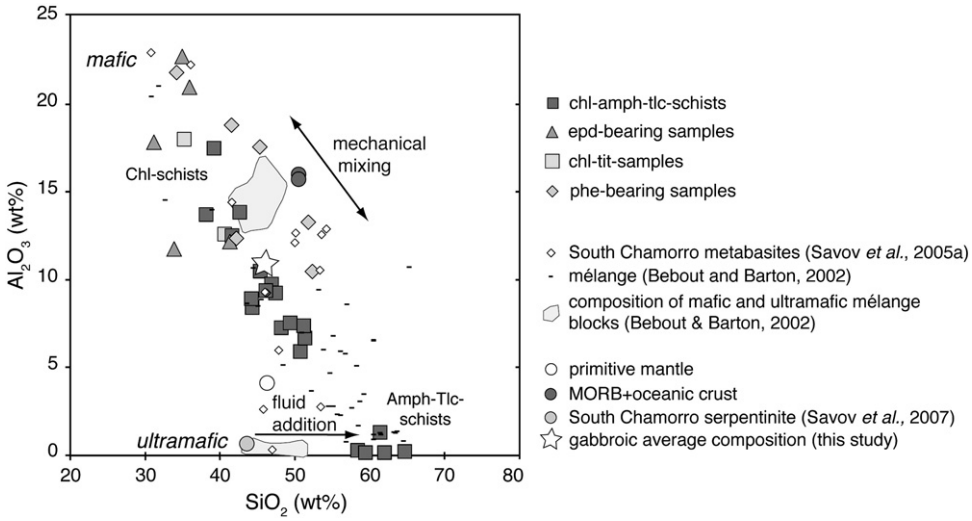

Fig. 5. Chemical discrimination diagram, MgO vs. Al_2O_3, calculated H_2O-free, demonstrating the conceptual model for mixing in the Mariana subduction mélange zone. The small white diamonds are South Chamorro Seamount metabasite compositions given by Savov et al. (2005a, 2005b). Large filled circles are MORB and oceanic crust, mantle wedge serpentinite and primitive mantle compositions (Lyubetskaya and Korenaga, 2007; Savov et al., 2007; Smith et al., 1995). Arrows indicate the trends for fluid addition and mechanical mixing. Gray fields are mafic and ultramafic end-member compositions from Catalina Schist mélange, black lines present Catalina Schist mélange matrix compositions (Bebout and Barton, 2002).

that phengite and chlorite are the major carriers of B, with amphibole and other mineral phases from the investigated samples having relatively low Li and B contents.

4.2.2. SIMS

The light element compositions of blueschist-facies minerals are reported in Table 4 (and electronic appendix A1). The SIMS analyses

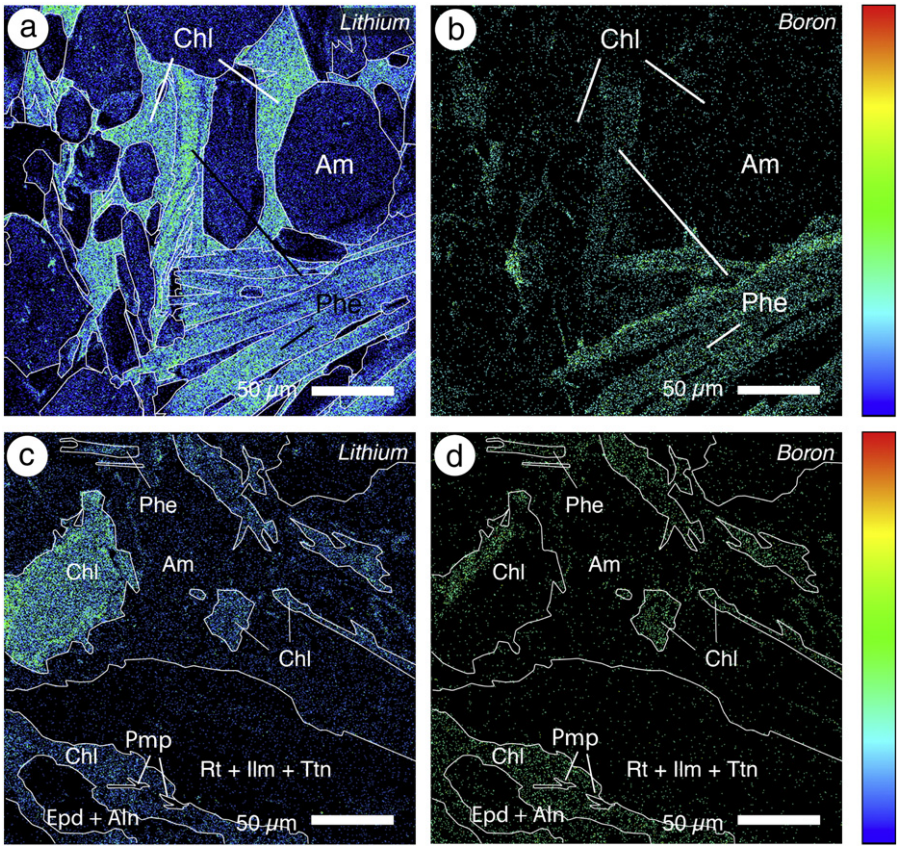

Fig. 6. ToF-SIMS element distribution maps of the lithium and boron distribution: a + b) sample E1H3-4d with chlorite, phengite and amphibole, c + d) sample E1H3-4b with Na-rich pyroxene (aegirin-augite: $Jd_{19}Ac_{41}Q_{40}$), Na-rich amphibole (winchite-richterite), chlorite and phengite sheaves in the upper left. Further minerals are Rt, Ttn, Ilm, Ep, Aln and Pmp. The contours indicate boundaries of mineral phases that were identified during electron microprobe analysis. The color scale to the right represents the number of ions counted (increasing from bottom to top), black = no counts. See Fig. 4 for mineral abbreviations.

Table 4
Light element concentrations (in μg/g) and boron isotope values (in ‰) of representative blueschist-facies minerals.

Analyses no.	Li (μg/g)	2σ	Be (μg/g)	2σ	B (μg/g)	2σ	δ^{11}B (‰)	δ^{11}B (‰)[a]	2σ
Allanite									
E1H3-4B-15	0.41	0.05	0.21	0.04	2.87	0.19			
F1H4-3A-2	0.40	0.04	1.01	0.13	17.47	0.88			
Epidote									
E1H3-4B-16	0.13	0.03	0.16	0.04	2.55	0.18	−2.45	−2.45	9.15
E1H3-4C-1	0.02	0.01	0.15	0.03	1.59	0.27	−15.56	−15.56	10.41
E4H2-2B-4	0.13	0.04	1.04	0.11	25.19	0.56	−10.17	−10.17	3.28
F1H4-3A-6	0.05	0.02	0.01	0.01	0.06	0.03			
F2H2-1A-4	0.01	0.01	0.18	0.07	0.25	0.09			
Pumpellyite									
E1H3-4B-10	3.41	0.16	7.19	0.42	19.84	0.61			
Amphibole									
D1H4-1A-13	1.43	0.29	0.47	0.04	1.94	0.17	−11.09	−8.09	10.30
D1H4-1A-3	3.19	0.17	0.72	0.05	3.54	0.12	−0.76	+2.24	9.60
D1H4-2D-11	0.08	0.01	2.82	0.24	6.45	0.25	−10.04	−7.04	7.44
D1H4-2D-13	0.13	0.02	6.63	0.31	10.99	0.32	−8.94	−5.94	6.18
D1H4-2D-15	0.09	0.02	2.04	0.51	4.74	0.21	−3.59	−0.59	6.80
D1H4-2D-5	0.10	0.03	2.03	0.13	7.73	0.30	−5.01	−2.01	7.98
D1H4-2D-9	0.07	0.02	6.00	0.33	23.32	0.74	−10.02	−7.02	6.98
E1H3-4A-2	1.95	0.09	0.74	0.07	7.39	0.29	−4.36	−1.36	6.10
E1H3-4A-14	12.90	0.67	0.46	0.04	3.32	0.21	−11.45	−8.45	4.94
E1H3-4A-1	13.71	0.32	0.70	0.07	5.75	0.18	−6.99	−3.99	6.48
E1H3-4A-3	15.89	1.34	0.44	0.13	2.50	0.19	−12.17	−9.17	5.24
E1H3-4B-1	8.34	0.29	3.26	0.19	4.37	0.27	−11.59	−8.59	4.52
E1H3-4B-3	8.54	0.29	3.56	0.11	4.73	0.26	−10.00	−7.00	4.48
E1H3-4B-6	9.41	0.18	4.06	0.15	3.18	0.25	−11.66	−8.66	5.00
E1H3-4B-18	7.37	0.14	3.03	0.09	3.91	0.25	−11.71	−8.71	5.23
E1H3-4D-14	17.32	0.37	1.91	0.09	3.31	0.27	−10.55	−7.55	6.53
E1H3-4D-15	12.04	0.24	0.16	0.01	2.07	0.11	−15.83	−12.83	1.90
E1H3-4D-16	18.61	0.38	1.38	0.09	3.49	0.23	−10.04	−7.04	5.57
E1H3-4D-34	3.93	0.09	1.57	0.09	2.64	0.24	−9.41	−6.41	6.83
E2H2-4J-2	0.02	0.01	0.06	0.02	3.17	0.23	−10.69	−7.69	9.94
F1H1-3E-1	5.63	0.20	1.03	0.13	2.80	0.32	−2.91	+0.09	10.48
F1H1-3F-1	0.04	0.01	0.36	0.08	6.49	0.33	−0.56	+2.44	6.82
F1H3-2C-2	0.04	0.01	1.51	0.28	4.03	0.30	−8.32	−5.32	9.68
F2H2-1A-1	0.44	0.07	0.88	0.13	2.36	0.19	−3.86	−0.86	10.84
F2H2-4A-6	1.84	0.15	0.36	0.07	3.72	0.35	−2.28	+0.72	9.2
F2H2-4B-1	1.22	0.15	1.10	0.10	3.05	0.19	−7.35	−4.35	10.74
F2H2-4B-4	7.31	0.22	3.48	0.16	3.85	0.28	−8.81	−5.81	8.56
F2H2-4H-1	1.57	0.09	2.01	0.14	3.15	0.25	−6.23	−3.23	9.60
F2H2-4H-4	1.80	0.00	3.51	0.00	2.19	0.00	−1.44	+1.56	8.98
F2H2-4J-2	1.30	0.12	0.52	0.06	2.80	0.29			
F2H2-5A-2	7.98	0.42	8.28	0.29	3.74	0.29	−3.66	−0.66	7.40
F2H2-5A-4	36.55	0.68	0.31	0.05	2.23	0.17	−1.03	+1.97	8.72
E7H2-1A-1	0.94	0.07	0.86	0.03	10.15	0.22			
E7H2-1B-1	1.76	0.14	0.78	0.08	7.72	0.50			
E7H2-2A-1	0.15	0.02	0.11	0.02	0.52	0.08			
Chlorite									
D1H4-1A-5	38.07	0.35	0.11	0.02	0.87	0.17	−0.89	+2.11	5.34
D1H4-2D-7	13.25	0.56	0.59	0.06	6.61	0.22			
E1H3-4A-4	72.33	0.84	0.26	0.05	1.30	0.11			
E1H3-4A-9	33.38	0.38	0.24	0.04	12.75	0.45			
E1H3-4B-2	99.59	1.10	0.12	0.02	1.03	0.15			
E1H3-4B-8	9.24	0.21	6.84	0.23	12.71	0.27	−3.66	−0.66	3.34
E1H3-4C-4	37.26	0.35	0.52	0.06	0.42	0.09			
E1H3-4D-31	58.34	0.39	0.24	0.04	4.53	0.42	−9.07	−6.07	1.39
E1H3-4D-18	73.39	0.76	0.14	0.04	0.39	0.06	−10.62	−7.62	1.41
E4H1-2A-3	4.02	0.25	0.02	0.01	17.16	0.65	+4.88	+7.88	4.18
E4H1-2A-6	4.71	0.17	0.02	0.01	5.54	0.45	−0.80	+2.20	7.92
E4H2-2B-5	48.42	1.85	0.33	0.06	1.47	0.08	−0.89	+2.11	8.98
E4H2-2B-7	49.51	0.68	0.38	0.06	3.52	0.40	−1.08	+1.92	7.88
F1H1-3E-3	140.00	2.78	0.01	0.01	2.29	0.27	−0.96	+2.04	7.94
F1H3-2C-4	7.90	0.49	0.11	0.07	15.42	1.08	−6.62	−3.62	7.50
F1H3-2D-2	17.14	0.39	0.27	0.06	17.36	0.42	−7.93	−4.93	3.56
F1H4-3A-5	79.92	1.23	0.25	0.04	0.93	0.11			
F2H2-1A-2	1.11	0.14	0.50	0.09	1.18	0.15	−10.7	−7.70	8.30
F2H2-4D-3	10.73	0.24	0.01	0.01	10.54	0.55			
F2H2-4F-1	23.21	0.54	0.14	0.04	1.94	0.45	−15.78	−12.78	10.58
F2H2-4G-2	35.42	0.59	0.16	0.05	1.71	0.48	−16.96	−13.96	8.68

(continued on next page)

Table 4 (*continued*)

Analyses no.	Li (μg/g)	2σ	Be (μg/g)	2σ	B (μg/g)	2σ	δ^{11}B (‰)	δ^{11}B (‰)[a]	2σ
F2H2-5A-3	10.23	0.32	0.02	0.01	8.42	0.44	+1.86	+4.86	6.44
Phengite									
E1H3-4A-7	66.82	1.10	1.84	0.08	41.52	0.92	−8.72	−5.72	1.39
E1H3-4A-12	62.16	2.71	1.70	0.15	40.89	0.31	−10.77	−7.77	1.45
E1H3-4A-13	76.85	0.62	2.00	0.12	37.91	0.62	−8.43	−5.43	1.49
E1H3-4B-14	83.78	2.51	2.88	0.09	36.98	0.66	−9.54	−6.54	1.79
E1H3-4D-30	78.67	0.67	1.57	0.07	43.32	0.46	−5.61	−2.61	1.33
E1H3-4D-23	94.19	1.38	1.05	0.07	35.65	0.49	−9.01	−6.01	1.53
E1H3-4D-24	96.79	1.03	1.01	0.08	36.99	0.52	−10.40	−7.40	1.46
E1H3-4D-2	97.19	0.52	1.96	0.11	41.27	0.66	−9.98	−6.98	2.52
E1H3-4D-4	100.90	1.05	1.37	0.10	34.72	0.84	−8.19	−5.19	2.14
E1H3-4D-29	105.35	0.55	1.78	0.07	29.31	0.62	−7.41	−4.41	1.43
F2H2-4H-2	35.41	1.32	1.32	0.11	45.04	0.69	−6.96	−3.96	2.66
F2H2-4B-2	39.00	1.48	1.06	0.06	34.80	0.79	−8.89	−5.89	2.14
F2H2-4A-3	39.45	1.19	0.79	0.07	29.98	0.87	−12.30	−9.30	2.40
F2H2-4A-5	42.98	0.46	0.80	0.08	32.10	0.67	−6.81	−3.81	2.60
F2H2-4B-6	50.89	1.56	1.34	0.13	37.86	1.03	−7.89	−4.89	2.42
F2H2-4H-5	53.81	0.66	3.02	0.22	33.63	0.95	−6.52	−3.52	2.72
F2H2-4B-3	56.39	1.41	1.93	0.20	36.42	1.35	−4.96	−1.96	2.40
F2H2-5A-1	26.98	1.38	1.31	0.10	49.74	0.86	−9.91	−6.91	1.94
F2H2-5A-5	37.46	0.53	1.54	0.13	40.09	0.85	−3.94	−0.94	2.46
Talc									
E2H2-5D-04	9.16	0.19	0.23	0.07	9.23	0.92			
Pyroxene									
F2H2-5A-6	2.49	0.00	1.08	0.00	13.37	0.00	+1.26	+1.26	3.84
F2H2-4H-3	1.19	0.08	0.24	0.04	3.73	0.37	−0.77	−0.77	7.98
Garnet									
E1H3-4C-3	4.38	0.15	0.00	0.00	0.06	0.02			

[a] Matrix corrected boron isotope values.

corroborate the ToF-SIMS imaging results, which show that phengite and chlorite are the major Li- and B-bearing phases (Fig. 7). The major Be carrier in the metamafic rocks embedded in Mariana forearc serpentine mud of SCS are amphibole, chlorite and pumpellyite (Table 4; Fig. 7b). In detail, pumpellyite has a very high Be concentration (7.2 μg/g) similar to the highest contents in amphibole and chlorite (Fig. 7).

Amphibole has variable Li and B concentrations with Li contents reaching ~40 μg/g and B reaching ~20 μg/g. Chlorite has similar B concentrations compared to amphibole (0.2–11 μg/g), but higher Li contents that reach up to 105 μg/g. Talc is enriched in both Li and B (~10 μg/g). Phengite compositions plot in a relatively distinct field in the Li-B co-variation diagram (Fig. 7) with 30–120 μg/g Li and 20–70 μg/g B. Sodic pyroxene has Li concentrations of about 2 μg/g and variable B concentrations (range = 3.7–13.4 μg/g). Epidotes from one clast (E4H2-2B) are strongly enriched in B (>8 μg/g). All other epidotes have low B (0.06–2.55 μg/g) and Li (0.004–1 μg/g) contents, with one exception in sample E4H2-2B (where Li = 5.5 μg/g). Pumpellyite (one analysis) has a high B content (19.8 μg/g) similar to the highest B measured in amphibole and chlorite, the Li concentration is 3.4 μg/g. Zoned garnet in association with epidote, titanite, apatite and chlorite (sample E1H3-4c) can be B-depleted while Li-rich (4.4 μg/g).

4.2.3. Bulk light element composition

It is obvious that the Li, Be and B contents are strongly controlled by their major carrier and rock-dominating minerals phengite, chlorite and amphibole (see Tables 4 and 5). Estimated bulk concentrations of these light elements range from <1 to 71 μg/g Li, 0.04 to 2.78 μg/g Be and <1 to 33 μg/g B. The average composition of the recovered metamafic clast inventory (without considering the relative abundance of rock types) is roughly ~23 μg/g Li, ~0.73 μg/g Be and ~8 μg/g B, which is in good agreement with the bulk rock Li and B compositions of similar metamafic fragments from SCS reported in Savov et al. (2005a; Fig. 8). However, the calculated B concentrations are lower when compared with the bulk rock values reported in Savov et al. (2005a). On the other hand, a higher number of Li- and B-rich samples clearly shows that more phengite-rich and weak samples could be recovered, i.e. were investigated in the present study due to cautious clast picking and preparation.

4.2.4. Boron isotopes

The B isotope analyses by SIMS (Table 4 and electronic appendix A1) show that B-rich phengites from different samples define a narrow range between −2 and −10‰ δ^{11}B, averaging at −6 ± 4‰ (Fig. 9). Predominantly, δ^{11}B values of amphibole, chlorite, pyroxene and epidote minerals with B concentrations of >10 μg/g (i.e., small 2σ errors) confirm this distinct boron isotope range (with one exceptional chlorite). When B concentrations are low, analytical errors increase, but even in such cases >80% of all minerals measured fall into the same δ^{11}B range (−2 and −10‰).

5. Discussion

5.1. New constraints on PT-conditions

The samples investigated in this study provide additional constrains on the pressure (*P*) and temperature (*T*) conditions of metamorphism in the Mariana forearc. Previous *PT* calculations for metamafic fragments recovered at several seamounts in the Mariana forearc were *T* = 150–250 °C and *P* = 0.5–0.6 GPa (Maekawa et al., 1992), equivalent to depths of 16 to 21 km below seafloor (Maekawa et al., 1992, 1993). Pyroxene of metamafic fragments from our SCS samples reach ~33% jadeitic component (Jd). This value coincides with mineral compositions given by Maekawa et al. (1992) and confirms their *PT* estimations made for metamafic rocks recovered from the Conical Seamount, ~1000 km to the north of SCS.

Seismic studies (Oakley et al., 2008) and geochemical fingerprints of clasts and fluids (e.g., Mottl et al., 2004; Savov et al., 2005a) strongly supports the idea that the metamafic materials from SCS are direct samples from the downgoing Pacific plate at depths of ~27 km (Fryer et al., 2000, 2006; Mottl et al., 2003). This is also consistent with

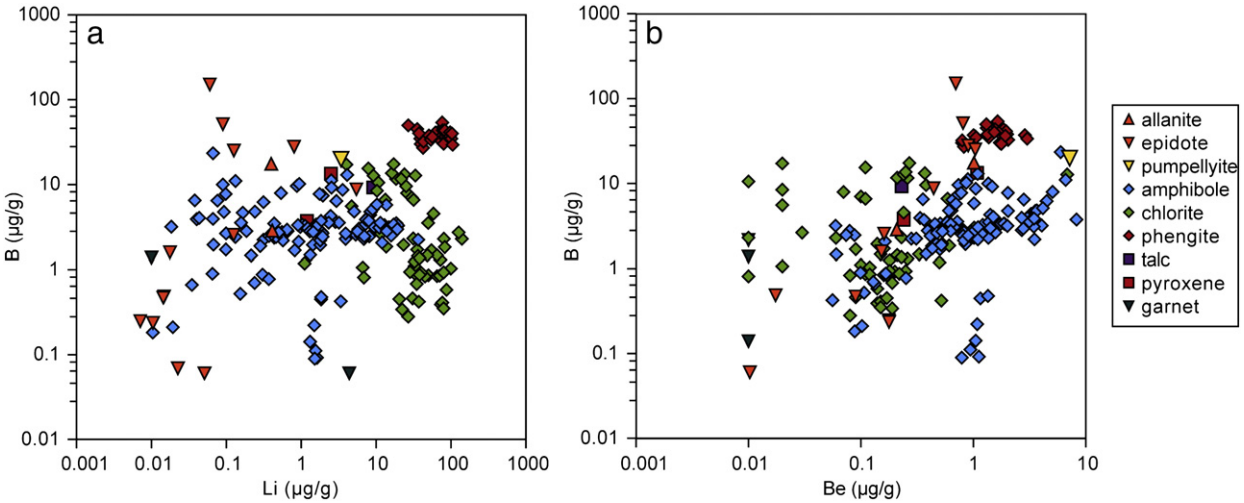

Fig. 7. a) Li vs. B content and b) Be vs. B content of minerals discovered in slab-derived blueschist facies clasts. Phengite is the major B carrier, phengite and some chlorite are the major Li carrier. Amphibole and phengite are the major Be hosts.

subduction-related earthquake locations that infer a slab depth of 29 km below Conical Seamount (Hussong and Fryer, 1982; Seno and Maruyama, 1984). For SCS Fryer et al. (2000) suggested *T* of up to 350 °C and *P* of ~0.8 GPa, equivalent to slab depths of ~26 km.

These two well-studied seamounts, South Chamorro and Conical Seamount, have a similar position relative to the subduction trench but at two spatially remote sites (Fig. 1b). Hence, it is important to note that *PT* conditions of the Mariana forearc are now not constrained based on a single site that could be an anomaly, but rather that the *PT* conditions within the same subduction zone remain the same for the shallow fluid-expelling regions. It is then expected that the subducting slabs in the Marianas will dehydrate in the same manner considering the subduction assemblage remains the same (old Pacific oceanic crust).

Our study documents the existence of pumpellyite (sample E1H3-4b) in (i) association with titanite, magnetite, rutile, ilmenite and epidote surrounded by a chlorite + (Na)–amphibole (±Na-Px) matrix, and (ii) single pumpellyite crystals in amphibole (also sample E1H3-4b). The comparative study of onland pumpellyite-bearing metamorphic terranes by Brown (1977) gives a petrogenetic grid

Table 5
Bulk rock composition (wt.%) of blueschist-facies clasts calculated after estimated mineral vol.%.

Sample	SiO_2	TiO_2	Al_2O_3	Cr_2O_3	Fe_2O_3	MnO	MgO	CaO	Na_2O	K_2O	NiO	P_2O_5	H_2O	Total	$Na_2O + K_2O$	Mg#	Li (µg/g)	Be (µg/g)	B (µg/g)
D1H4-1a	48.79	0.02	6.29	0.15	12.64	1.21	20.65	3.60	2.35	0.03	0.10	0.00	4.16	95.84	2.38	62.12	12.80	0.49	3.19
D1H4-2d	40.58	2.47	8.05	0.01	9.12	0.22	24.47	6.56	0.35	0.04	0.15	0.66	7.33	92.67	0.39	74.36	7.78	1.22	5.21
D3H1-8C	38.58	0.07	11.15	0.49	7.46	0.04	29.37	0.69	0.22	3.92	0.26	0.00	7.75	92.25	4.13	81.28			
E1H3-3d	33.31	0.36	11.77	0.01	11.28	0.24	28.29	2.26	0.34	0.09	0.08	0.82	11.14	88.86	0.43	73.10	20.60	0.41	10.64
E1H3-4a	38.87	1.10	17.35	0.05	14.38	0.28	13.03	3.24	1.08	3.80	0.03	1.64	5.15	94.85	4.88	49.61	51.92	0.97	18.23
E1H3-4b	39.12	5.01	11.30	0.14	13.88	0.32	15.94	8.16	1.64	0.16	0.04	0.00	4.30	95.70	1.80	55.40	22.70	2.78	4.84
E1H3-4c	28.84	1.89	16.28	0.10	14.92	1.91	12.62	13.06	0.23	0.01	0.10	4.10	5.93	94.07	0.24	45.11	22.91	0.23	0.88
E1H3-4d	42.85	1.46	16.40	0.14	11.31	0.41	13.50	4.98	1.31	2.99	0.05	0.00	4.60	95.40	4.30	56.02	48.90	1.23	13.77
E1H3-5	40.33	0.01	9.20	0.25	6.23	0.20	29.37	3.82	0.06	0.01	0.17	0.00	10.36	89.64	0.07	83.49			
E2H2-4b	37.67	0.41	11.12	0.03	12.45	0.17	25.25	4.13	0.21	0.07	0.08	0.41	8.00	92.00	0.28	68.91			
E2H2-4j	58.69	0.00	0.04	0.03	3.72	0.10	22.52	13.29	0.23	0.05	0.04	0.00	1.29	98.71	0.28	86.72	0.26	0.07	2.46
E2H2-5d	48.41	0.05	6.82	0.23	8.39	0.51	23.40	5.62	0.64	0.03	0.18	0.82	4.90	95.10	0.67	74.36	13.61	0.72	4.40
E2H2-5j	60.45	0.02	0.13	0.10	3.41	0.01	29.30	0.00	0.03	0.00	0.34	0.00	6.20	93.80	0.04	90.49			
E4H1-2a	40.97	0.21	8.15	0.07	9.67	0.15	23.90	6.28	0.41	0.02	0.14	0.00	10.01	89.99	0.43	72.94	2.65	0.04	4.70
E4H2-2b	32.74	0.81	20.98	0.02	15.65	0.28	8.51	15.25	0.01	0.00	0.03	0.82	4.89	95.11	0.01	37.17	20.17	0.61	32.91
E7H2-1a,b,2a,8a,b,10	45.88	0.93	6.76	0.03	11.23	0.41	19.66	9.12	0.99	0.05	0.09	0.82	4.01	95.99	1.04	65.11			
E7H2-6A	30.11	1.09	15.13	0.03	14.64	0.45	25.27	1.03	0.08	0.01	0.00	0.00	12.15	87.85	0.09	64.95			
F1H1-3C	44.18	0.02	8.47	0.50	8.72	0.38	24.83	6.21	0.28	0.02	0.24	0.00	6.13	93.87	0.30	75.08			
F1H1-3D	30.10	0.01	18.95	0.00	14.93	0.59	25.31	0.01	0.01	0.30	0.04	0.00	9.76	90.24	0.31	64.32			
F1H1-3E	41.71	1.63	7.75	0.13	7.23	0.45	20.35	10.26	0.70	0.03	0.14	1.64	7.99	92.01	0.74	74.52	70.85	0.29	2.46
F1H1-3F	45.07	0.03	6.75	0.12	10.10	0.20	24.98	6.57	0.76	0.03	0.19	0.00	5.20	94.80	0.79	72.87	8.20	0.34	9.11
F1H3-2C	57.84	0.01	1.18	0.03	3.55	0.14	29.20	2.08	0.08	0.01	0.43	0.00	5.45	94.55	0.09	89.75			
F1H3-2D	35.57	3.08	10.87	0.01	10.53	0.08	25.59	2.85	0.14	0.09	0.05	0.00	11.12	88.88	0.23	72.79	16.05	0.45	20.01
F1H3-2F	57.94	0.01	0.10	0.02	2.63	0.12	28.07	4.27	0.19	0.01	0.25	0.00	6.37	93.63	0.20	91.83			
F1H4-3a	32.66	1.02	18.82	0.01	12.75	0.56	18.80	7.68	0.02	0.01	0.03	0.00	7.64	92.36	0.03	60.96	66.59	0.39	1.32
F1H4-5	42.78	0.01	8.71	0.45	6.67	0.30	26.77	5.59	0.29	0.02	0.27	0.00	8.16	91.84	0.30	80.94			
F2H2-1A	31.89	0.42	10.89	0.02	12.68	0.77	10.33	18.90	0.92	0.06	0.06	8.20	4.85	95.15	0.99	45.86	0.57	0.60	1.34
F2H2-3F	57.12	0.01	0.15	0.06	7.14	0.14	20.47	12.02	0.54	0.07	0.29	0.00	1.99	98.01	0.61	75.68			
F2H2-4A,B,H	49.80	1.34	12.55	0.03	12.08	0.35	10.41	3.67	2.44	4.12	0.01	0.00	3.20	96.80	6.56	48.09	21.28	1.72	16.94
F2H2-4D	48.20	0.11	5.49	0.15	9.75	0.17	22.04	9.31	0.18	0.02	0.07	0.00	4.51	95.49	0.20	71.12	3.60	0.09	4.94
F2H2-4E,G, 5G	37.83	0.10	12.22	0.26	8.04	0.49	27.34	2.98	0.12	0.01	0.19	0.21	10.23	89.77	0.13	77.94	27.59	0.29	1.45
F2H2-4F,J	34.46	0.03	15.31	0.22	7.60	0.43	29.37	1.19	0.07	0.01	0.22	0.00	11.09	88.91	0.07	80.14	21.96	0.23	1.23
F2H2-5A	50.52	1.12	9.93	0.04	12.09	0.48	13.45	4.50	2.72	2.35	0.02	0.00	2.77	97.23	5.07	54.19	22.50	2.10	14.97

Bulk rock compositions (wt.%) calculated after estimated mineral vol.%. Mg# = 100*MgO/(MgO + MnO + FeO). Totals exclusive H_2O.

for relative *PT*-range estimations. Although the limiting phase relationships require quartz and albite, which do not occur in the pumpellyite-bearing sample from South Chamorro Seamount, the Black Butte blueschist in the Franciscan Complex includes the critical phase assemblage Pmp + Ep + Na-Am. Tectonically, the Franciscan Complex represents mélange units including blueschist-facies rocks that were emplaced in forearc position (e.g., Bebout et al., 1993; Cloos, 1986; Grove and Bebout, 1995; King et al., 2007). Temperatures for these Franciscan pumpellyite-bearing blueschists are in the range 250–300 °C at pressures of ~0.7 GPa (Brown and Ghent, 1983). Accordingly, the pumpellyite-bearing sample from SCS can confirm the published *PT* estimates and seismic observations at both Conical and South Chamorro Seamounts for the Mariana forearc region.

5.2. Composition of the subducted Pacific slab under the Mariana forearc and evidence for a subduction mélange

The metamafic rock types recovered from SCS (and other serpentinite seamounts on the Mariana forearc) present a great variety of lithologies that appear to be ripped off pieces of the subducting Pacific slab that became incorporated into the fault gouge, which assisted the exhumation of these clasts via serpentinite mud volcanism (e.g., Cloos and Shreve, 1996; Fryer et al., 2006; Mottl et al., 1998; Sample and Karig, 1982; Scholz and Small, 1997; Shipley et al., 1992; Yamazaki and Okamura, 1989). The compositional range between samples in the present study suggests a relevant heterogeneity of the exhumed solid slab materials. Although the metamafic clasts erupted by the SCS cannot give any information about their original spatial relationship, they show a very similar lithology and geochemical composition compared to exposed onland mélange outcrops.

Such tectonic mélanges are among the most characteristic features of subduction zones found in forearc regions with various ages and tectonic histories (e.g., Bebout and Barton, 1989, 2002; Bebout et al., 1993; King et al., 2006). At these settings, the mélange rocks are characterized by chaotic hybridized mixtures of peridotites, basalts and sediments that have experienced blueschist-, amphibolite-, or eclogite-facies metamorphic conditions (e.g., Bebout and Barton, 1989, 2002; Bebout et al., 1993; Fisher, 1996; King et al., 2003, 2006). Bulk compositions vary between oceanic (MORB-type) basalts and peridotites (Altherr et al., 2004; King et al., 2007; Marschall et al., 2007), represented by variously serpentinized regions mixed with metamorphic schist-assemblages and tectonic blocks affected by strong mechanical mixing, deformation and metasomatism due to fluid flow (e.g., Bebout and Barton, 1989, 2002; Breeding et al., 2004; King et al., 2006; Sorensen and Grossman, 1989). The formation of such mélange zones along the slab–mantle shear zone is enabled by the presence of rheologically weak minerals above the subducting slab, formed during slab devolatilization and the resulting fluid-rock interactions (Bebout and Barton, 1989, 2002; Bebout et al., 1993; Peacock and Hyndman, 1999; Reinen, 2000; Reinen et al., 1994).

Observations and geochemical studies on high-pressure metamorphic rocks and adjacent serpentinites in mélange suites are based on onland locations where erosion has exposed ancient subduction zones accompanied by retrograde metasomatism, such as the Franciscan Catalina Schist (USA), Syros (Greece) and Elekdag (Turkey) (Altherr et al., 2004; Bebout, 1995; Breeding et al., 2004; Coleman and Clark, 1968; Essene and Fyfe, 1967; King et al., 2006; Marschall et al., 2006a, 2007; Miller et al., 2009; Pelletier et al., 2008; Sorensen and Grossman, 1989). Direct sampling of an active slab–mantle interface is possible only in the Mariana subduction zone.

Fig. 5 shows the SiO_2-Al_2O_3 variation of SCS metamafic rocks (this study; Savov et al., 2005b) compared to amphibolite-grade (0.8–1.1 GPa; 640–750 °C) mélange rocks from the Catalina Schist, California (Bebout and Barton, 2002), where chemically distinct 'endmember'-groups and 'rind'-groups associated to slab–mantle-interaction were described (Bebout and Barton, 1989; Bebout et al., 1993; Breeding et al., 2004; King et al., 2003; Manning, 1997; Marschall, 2005; Miller et al., 2009; Sorensen and Grossman, 1989). Very similar compositions are found for the SCS rocks indicating that they are hybridized mélange originating clasts.

In detail, serpentinized mantle peridotite with an average composition of 43 wt.% SiO_2 and Mg# of 91–93 (Savov et al., 2005a,b, 2007) makes the ultramafic endmember within the Mariana subduction mélange. Associated 'rind metasomatism' is indicated by a decrease of MgO and increase of SiO_2 contents at constant Al_2O_3 and the formation of talc-rich rocks with tremolitic to actinolitic amphibole (Fig. 5). Talc abundance decreases and chlorite becomes the major phase together with amphibole with distance to the serpentinite.

The mafic 'endmember', i.e., the subducted and metamorphosed Pacific oceanic slabs under the Mariana forearc, is transformed into epidote-bearing rocks which are enriched in Al_2O_3 and CaO, but relatively depleted in SiO_2 (Table 5; Fig. 5). Accordingly, phengite-rich amphibole-chlorite-schists represent the meta-sedimentary portion of this subducting Pacific slab inventory. These rocks are enriched in Al_2O_3, Na_2O and K_2O, but have low CaO (Table 5). Samples with predominantly chlorite and little phengite might be metasomatic 'rinds' related to these meta-sediments. Metasomatic 'rind' formation associated with mafic (both epidote- and phengite-rich samples) rocks is characterized by decreasing Al_2O_3 and increasing SiO_2 concentrations (Fig. 5) related to an increase in amphibole and talc abundance.

In the Catalina Schist and Syros subduction complexes, the mélange matrix is composed of weak material formed by mechanical and geochemical mixing processes. Such mélange material from the Mariana slab–mantle-interface might probably be disaggregated in the uprising fluid-serpentine-mud mixture or represented by some fine-grained chlorite-amphibole-schists. Evidence for such tectonic mixing is indeed given by a strongly foliated sample of chlorite intergrown with biotite and tiny andradite and spinel grains concentrated in the chlorite and clasts of intergrown chlorite and titanite.

The geochemical variation with strong tendencies of mechanical and fluid-driven mixing of the SCS samples (Fig. 5) shows that metasomatism along the slab–mantle boundary is an important mechanism. Hence, assumptions about fluid fluxes and calculations of element loss due to dehydration during subduction must be interpreted in a critical manner.

Some epidote-schists from SCS show the presence of garnet. This matches the high pressures acquired only in the forearc, as garnet is not a direct slab component. Altogether, even at shallow depths, what is thought to be a stratified sediment-MORB-peridotite, slabs are disintegrated already and represented by a complex fine grained mix. If this is the case, it is important for fluid mechanics, since the media is more porous and reaction surfaces are much larger (e.g., Ague, 2007). Hence, elemental fluxes will be larger and exchanges would be maximized early on in the subduction process.

5.3. Fluid and light element loss during shallow subduction

This study presents new insights about the Li, Be and B distribution between minerals from metamafic clasts from an active subduction zone. As expected in such lithologies, chlorite is the major phase for Li and phengite the major phase for B (see e.g., Domanik et al., 1993; Marschall et al., 2006a). However, it is noteworthy that chlorite can also be a major host for B, as observed in several samples by SIMS and ToF-SIMS (Fig. 6d).

The 'reconstructed' bulk rock light element concentrations of theSCS metamafics vary strongly from nearly zero to ~70 μg/g (for Li) and ~35 μg/g (for B) (Fig. 8) and average bulk rocks are estimated to contain ~23 μg/g Li, ~0.73 μg/g Be and ~8 μg/g B. Similar light element concentrations and low B/Be ratios (<30) were observed for blueschist-facies meta-sedimentary rocks from the Catalina Schist (~10–41 μg/g Li, ~0.2–1.4 μg/g Be and ~8–59 μg/g B; Bebout et al., 1993, 1999). The protolith of the metamafic rocks is the subducting

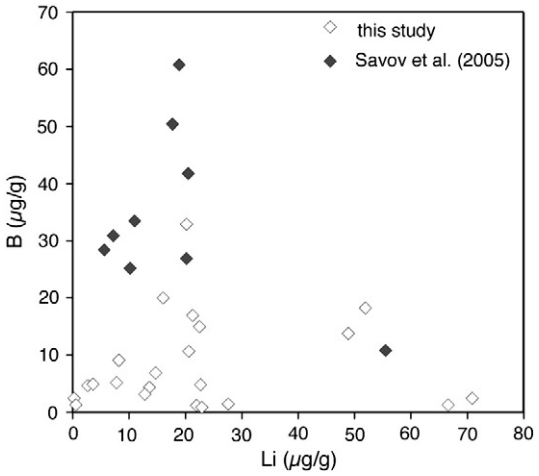

Fig. 8. Li vs. B of estimated bulk rock concentrations compared to bulk rock compositions of metamafic fragments from Conical and South Chamorro Seamounts studied by Savov et al. (2005a).

Pacific plate which experienced low *T* seawater alteration resulting in an enrichment in light elements compared to depleted mantle (Bonatti et al., 1984; Deschamps et al., 2011; Kelley et al., 2003; Salters and Stracke, 2004; Sano et al., 2004; Spivack et al., 1987; Thompson and Melson, 1970; Vils et al., 2008, 2011). Oceanic crust at IODP 1256D has B contents of ~1 to 6 µg/g (Sano et al., 2008) and altered crust at ODP Site 801 in the Western Pacific has Li concentrations of about 3–97 µg/g and Be concentrations of about 0.05–3.1 µg/g (Kelley et al., 2003). The composition of pelagic sediments is about 2 to 96 µg/g Li, 0.3 to 2.8 µg/g Be and about 15 to 132 µg/g B (Ishikawa and Nakamura, 1993; Ryan and Langmuir, 1988). However, sediment input is limited due to the very thin sediment pile that is actually subducted at the Marianas Trench (e.g., Stern et al., 2003 and references therein). Nevertheless, it can be expected that the hydrous portion of the subducting slab introduces large amounts of Li (Be) and B into the otherwise light element poor deep mantle regions (depleted mantle: 0.7 µg/g Li, 0.0025 µg/g Be and 0.06 µg/g B; Salters and Stracke, 2004). The bulk rock light element abundances of the metasomatized SCS metamafic rocks are variable but in average lower than in the subduction input of average altered oceanic crust (AOC; ~15 µg/g Li and ~0.8 µg/g Be: Kelley et al., 2003 and ~26 µg/g B: Smith et al., 1995) plus sediments that arrive at the Marianas Trench implying Li-, Be- and B-loss by dehydration during subduction until 27 km depth below SCS. As expected, Be appears to behave less fluid mobile than B. The low B/Be ratio implies that B was preferentially removed from the slab during early subduction while Be concentrations hardly changed. Savov et al. (2007) report large slab inventory depletions of ~75% for B and ~15% for Li based on Mariana forearc samples recovered at Conical and South Chamorro Seamounts. The limited Be mobility recorded by SCS rocks correlates with the low temperature alteration environment (Maekawa et al., 1992, 1993; Vils et al., 2011). However, the significant light element concentrations in the mélange zone derived SCS metamafic rocks propose that still large amounts of Li, Be and B, bound in minerals such as chlorite, amphibole, phengite and epidote, are carried in the subducting Pacific slab for further subduction in the Marianas.

5.4. Boron isotope evolution of the Mariana slab

The δ^{11}B ratios in the B rich SCS metamafic rocks have an average value of −6‰ ±4‰. Unmodified mantle peridotites and MOR volcanic rocks show low to extremely low light element (Li, Be, B) concentrations (Ryan and Langmuir, 1987, 1988, 1993). To the contrary, subducting sediments, altered (serpentinized) oceanic crust and serpentinized ultramafic rocks (mantle wedge) are important reservoirs for light elements such as B and show δ^{11}B values higher than MORB (or depleted mantle reservoir), due to a preferential enrichment of the heavy isotopes during the interaction with seawater or B-rich slab-derived fluids (Bonatti et al., 1984; Chan et al., 2002; Vils et al., 2008, Vils et al., 2009). The altered oceanic crust (AOC) has been shown to be the major B contributor to the subarc mantle. Its isotope composition can vary between −4‰ and +25‰, depending on the mineralogy, extent of fluid-rock interactions, temperature, pressure and pH experienced by the slabs during low *T* seafloor metamorphism (Oman and Cyprus ophiolites; Smith et al., 1995; Foustoukos et al., 2008). While the average boron isotopic composition of AOC is reported as +3.4 ±1.1‰ (Smith et al., 1995), the B isotope signature of seafloor pelagic sediments ranges from −7 to +11‰ (Ishikawa and Nakamura, 1993). Volumetrically subordinate trench turbidites have δ^{11}B values between −6 and −1‰ (You et al., 1995). These data suggest that the average δ^{11}B value of the altered Pacific crust is slightly positive (Fig. 10) in agreement with Smith et al. (1995). Consequently, the consistently negative δ^{11}B value of −6‰ in SCS blueschist-facies metamafic minerals implies release of ^{11}B-enriched aqueous fluids from the subducted slab inventory during progressive slab devolatilization and metasomatism due to subduction zone metamorphism. The dataset we report in this study is in agreement with existing reports for rocks recovered from active subduction zone studies that reported a δ^{11}B value of −8 or −10‰ for subducted sediments (Ishikawa and Tera, 1997; Smith et al., 1997), −3 to −7‰ for metabasalt that experienced subduction zone metamorphism (Peacock and Hervig, 1999) and −2 to −9‰ for blueschist-facies metasomatized rocks from the Catalina Schist (Bebout et al., 1992, 1999; King et al., 2007).

King et al. (2007) modeled the B isotope fractionation during progressive dehydration of subducting oceanic crust and used a δ^{11}B of +3.4‰ (Smith et al., 1995) for AOC as a starting value. The same approach can be applied for the Mariana subduction zone system (Fig. 10). The preferential loss of the heavier isotope ^{11}B during Rayleigh fractionation results in a heavier δ^{11}B in the fluid fraction and a lighter δ^{11}B in the residual subducting slab material (Benton et al., 2001; Leeman and Sisson, 2002; Palmer and Swihart, 1996; Peacock and Hervig, 1999; Rosner et al., 2003; Ryan, 2002; Savov et al., 2004; Williams et al., 2001). Considering a temperature of 300–350 °C at ~27 km as the depth of the slab–mantle-interface, an experimentally determined B isotope fractionation value (Δ^{11}B) between boromuscovite and fluid of −14.8 and −13.3‰ (stronger fractionation at lower temperature) can be applied (Wunder et al., 2005). This is in agreement with an experimentally derived isotope fractionation factor of B between silicates ($B^{[4]}$) and water ($B^{[3]}$) between −15.2 and −13.8‰ at 300 and 350 °C, respectively (Williams et al., 2001). At very low *T* (~200 °C) a fractionation (Δ^{11}B) of even −21‰ is expected between sheet silicates and fluids of neutral to basic pH (Williams et al., 2001; Wunder et al., 2005).

Thereafter, the decreasing fractionation factors with depth can change the δ^{11}B value of the slab material from about +3.4‰ down to the observed range of −10 to −2‰ below SCS (Fig. 10). Our new δ^{11}B mineral dataset is providing evidence that boron fractionation of subducted crust and sediments is already very effective at shallow depths of up to ~27 km in the Mariana subduction zone.

5.5. Boron isotope composition of slab-released fluids

Boron isotope values of fluids released from the subducting Pacific slab must respond to the fractionation behavior between slab material and fluid release during subduction. As the subducting altered oceanic crust has a positive δ^{11}B value (Smith et al., 1995), fluids released at the onset of dehydration, where temperatures are very low and B fractionation between silicates and fluids is large (Peacock and Hervig, 1999; Wunder et al., 2005), have positive δ^{11}B values, significantly above the ranges of mantle and MORB (Marschall et al.,

2007; You et al., 1995). With increasing depths and temperatures, the B fractionation factor between slab minerals and expelled fluid will decrease (Peacock and Hervig, 1999; Wunder et al., 2005). Fig. 10 shows how boron isotope ratios of minerals and released fluids decrease when subduction proceeds and that $\delta^{11}B$ of fluids can also reach negative values, even lower than those of the depleted MORB mantle. In our case, at the large temperature range of 200–350 °C in ~27 km depth below South Chamorro Seamount, a slab (amphibole, phengite, chlorite)-released fluid with a heavy $\delta^{11}B$ (max. +14 ±4‰) can be expected, leaving behind slab material with the observed light $\delta^{11}B$ (−6±4‰) (Fig. 10). If chlorite and amphibole with a slightly positive B isotope signature (Fig. 9) dehydrate, the corresponding fluid might reach $\delta^{11}B$ values in access of +20‰. Considering the heterogeneous nature of the mélange zones (i.e., well-documented large variations in the lithology, initial B and B isotope values) and in the metamafic clasts from SCS, in particular, it is reasonable to assume large chemical gradients of the expelled slab fluids produced via dehydration and metasomatic reactions occurring with depth and upon transit through the mantle to the surface.

The relatively low-temperature slab released fluids are available for the hydration of the overlying mantle wedge peridotite. The heavy B isotopic fluid signature (+14‰; Fig. 10) at slab depth very well explains the heavy $\delta^{11}B$ signature of upwelling fluids (+9 to +13‰) in the Mariana forearc region reported by Benton et al. (2001) for Conical Seamount and Savov et al. (2004) for SCS. This clearly supports the idea of a common deep fluid source for these fresh upwelling fluids most probably resulting from dehydration of various minerals from both the sediment and from the altered basalt (AOC) of the subducting Pacific Plate, as previously suggested by Mottl et al. (2003, 2004).

One consequence of the release of these B-rich slab-derived fluids is the metasomatic reworking of the dry and B poor depleted mantle wedge peridotites that overly the dehydrating subducted slabs (e.g., Pabst et al., 2011; Ryan and Langmuir, 1993; Savov et al., 2005b, 2007). In agreement with Benton et al. (2001), we argue that due to the B-free nature of the dry MORB mantle and the high pH of the hydration reactions, the serpentinization of the subarc mantle wedge should reflect well the original boron isotope signatures of the slab-derived fluid (~+14‰). Indeed, the Mariana mantle wedge serpentinites record a variable B enrichment (up to 40 μg/g, avg ~25 μg/g;

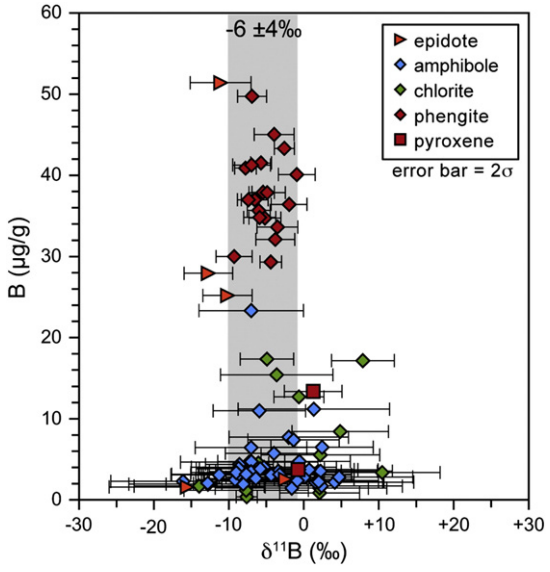

Fig. 9. B isotope ratios vs. B concentrations for phengite, chlorite and amphibole in blueschist facies clasts by SIMS analyses. The correlation shows that bulk blueschists average at about −6‰ $\delta^{11}B$, highlighted by gray field. Only data with 2σ errors of <11‰ are plotted, representing the analytically most confident data.

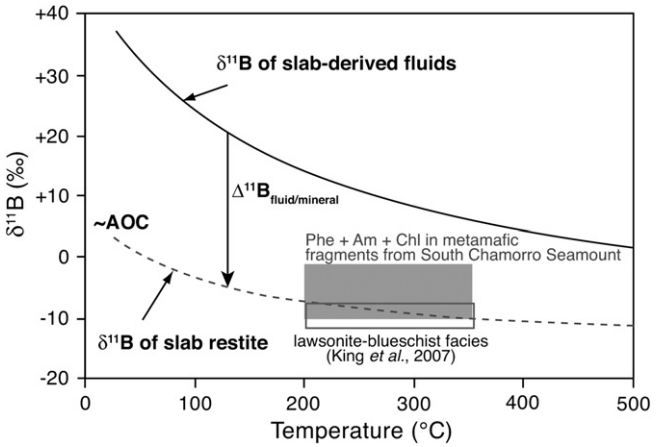

Fig. 10. The evolution of $\delta^{11}B$ as a function of temperature (=increase of fluid loss) for the metamafic minerals Phe, Am and Chl from South Chamorro Seamount, Mariana forearc (grey box) and comparison to the field of lawsonite-blueschist facies rocks from of the Catalina Schist (King et al., 2007). Figure modified from King et al. (2007), the temperature dependence of fractionation lines of the residual slab and slab-derived fluids were modeled by Peacock and Hervig (1999), Benton et al. (2001), Rose et al. (2001), Bebout and Nakamura (2003) and Rosner et al. (2003). AOC marks the approximate $\delta^{11}B$ of altered oceanic crust (+3.4±1‰; Smith et al., 1995).

Savov et al., 2007) and a wide range of $\delta^{11}B$ values in the serpentine minerals from −14‰ to +24‰ in (Pabst, 2009) and an average forearc bulk serpentinite $\delta^{11}B$ of ~+13‰ (Benton et al., 2001; Savov et al., 2004).

6. Conclusions

Metamafic rocks from SCS consist of dominantly amphibole-chlorite-schists, phengite-bearing schists and epidote-bearing rocks with a general lithology similar to onland mélange locations such as the Catalina Schist. Mineral assemblages recovered in the Mariana forearc region clearly indicate blueschist-facies conditions within a metasomatic mélange zone at slab depths of ~27 km. Our conclusions are in very good agreement with the results obtained by Maekawa et al. (1992, 1993) and Fryer et al. (2000, 2006) from studies of metamorphic conditions under the Conical Seamount located at similar to the SCS depth to the slab but located in the forearc region ~1000 km to the north. The 'pristine' metamafic material from the subducted Pacific crust and sediments, which has not been exposed to retrograde metamorphism, uplift and exposition onland, provides a strong support for experimental results of B-loss and B isotope fractionation with progressing subduction.

This study reveals that $\delta^{11}B$ values of the SCS blueschist-facies minerals are well defined between −10 and −2‰. This is a direct evidence that the Mariana forearc devolatilization reactions produce isotopically light residual slabs in comparison with the AOC (+3.4 ±1.1‰; Smith et al., 1995) and sediments (−7 to +11‰; Ishikawa and Nakamura, 1993). The negative $\delta^{11}B$ range can be well explained by Rayleigh fractionation between slab material and released fluids at low temperatures and is consistent with the current state of knowledge on light element cycling during ongoing and even ancient subduction zones processes (Agranier et al., 2007; Halama et al., 2009; Peacock and Hervig, 1999; Ryan et al., 1995).

On the one hand, the Mariana forearc slab-derived fluids must have a specific boron isotope composition, corresponding to the light $\delta^{11}B$ slab signature (e.g., Wunder et al., 2005). This isotopically light signature is expected to be reflected by subduction outputs such as serpentinite muds and is in agreement with known boron isotope data for Mariana mantle wedge serpentinites (~+13‰ (Benton et al., 2001; Savov et al., 2004). A more detailed picture upon specifics of the element fractionations within the Mariana forearc might be

provided by tracking the B and Li isotopes attached to single textural types of serpentine group minerals as common in mantle wedge serpentinites.

Some authors have already suggested links between light element recycling and the fate of deeply subducted oceanic slabs (Domanik et al., 1993; Straub and Layne, 2002; Tonarini et al., 2003; Zack et al., 2003). The still elevated Li, Be and B concentrations of the remaining slab materials bear a strong potential to further transport fluid-mobile elements to greater depths. We suggest here that the deep subduction of such forearc dehydrated and metasomatized lithologies may have impact on the chemical fingerprints of not only the arc magmas (e.g., Rose et al., 2001) but also to the deeply derived OIB magmatic suites and thus influence the still existing global imbalance for these fluid and melt mobile elements.

Continuing B fractionation during deeper subduction will further decrease the δ^{11}B of the subducted slab materials. Indeed, this scenario predicts well the relatively light δ^{11}B values for many island arc volcanic rocks that were produced in equilibrium with the mantle (primitive arc basalt suites, for example +4.5 to +12.0‰ in the Izu Arc; Ishikawa and Nakamura, 1994; Straub and Layne, 2002). It also postulates that arc front rocks that possess heavy δ^{11}B (up to +18‰ for South Sandwich and El Salvador lavas; Tonarini et al., 2007, 2011) must not be produced solely based on inputs from the subducting slabs, but also require the physical addition of forearc modified serpentinites as proposed by Benton et al. (2001), Savov et al. (2004, 2005b, 2007) and Tonarini et al. (2007, 2011).

Hence, the Mariana forearc metamafic rocks are a fundamental link between input materials (e.g., altered oceanic crust and sediments), deep subduction related lithologies such as eclogites, and output materials such as arc magmas.

Supplementary materials related to this article can be found online at doi:10.1016/j.lithos.2011.11.010.

Acknowledgements

This study is part of the PhD work of the first author, funded by grants from the Deutsche Forschungsgemeinschaft (DFG, #Za285/4). The samples were allocated to I. Savov by the Ocean Drilling Program (ODP Leg 195, Site 1200). ODP is sponsored by the U.S. National Science Foundation (NSF) and participating countries under the management of Joint Oceanographic Institutions (JOI), Inc. We like to thank H.P. Meyer for support with the electron microprobe analyses.

References

Agranier, A., Lee, C.-T.A., Li, Z.-X.A., Leeman, W.P., 2007. Fluid-mobile element budgets in serpentinized oceanic lithospheric mantle: insights from B, As, Li, Pb, PGEs and Os isotopes in the Feather River Ophiolite, California. Chemical Geology 245, 230–241.

Ague, J.J., 2007. Models of permeability contrasts in subduction zone mélange: implications for gradients in fluid fluxes, Syros and Tinos Islands, Greece. Chemical Geology 239, 217–227.

Alt, J., Honnorez, J., Laverne, C., Emmermann, R., 1986. Hydrothermal Alteration of A 1 km Section Through the Upper Oceanic Crust, Deep Sea Drilling Project Hole 504B: Mineralogy, Chemistry and Evolution of Seawater-Basalt Interactions. Geophysical Research 91.

Altherr, R., Topuz, G., Marschall, H., Zack, T., Ludwig, T., 2004. Evolution of a tourmaline-bearing lawsonite eclogite from the Elekdag area (Central Pontides, N Turkey): evidence for infiltration of slab-derived B-rich fluids during exhumation. Contributions to Mineralogy and Petrology 148, 409–425.

Bebout, G.E., 1995. The impact of subduction-zone metamorphism on mantle-ocean chemical cycling. Chemical Geology 126, 191–218.

Bebout, G.E., Barton, M.D., 1989. Fluid-flow and metasomatism in a subduction zone hydrothermal system: Catalina Schist terrane, California. Geology 17, 976–980.

Bebout, G.E., Barton, M.D., 2002. Tectonic and metasomatic mixing in a high-T, subduction-zone mélange–insights into the geochemical evolution of the slab–mantle interface. Chemical Geology 187, 79–106.

Bebout, G.E., Nakamura, E., 2003. Record in metamorphic tourmalines of subduction-zone devolatilization and boron cycling. Geology 31, 407–410.

Bebout, A.E., Graham, C.M., Leeman, W.P., Sisson, V.B., 1992. Trace element distribution and mobility during prograde metamorphism of sediments: ion-microprobe study of the Pelona schist, California. American Geophysical Union EOS 73, 327.

Bebout, G.E., Ryan, J.G., Leeman, W.P., 1993. B-Be systematics in subduction-related metamorphic rocks: characterization of the subducted component. Geochimica et Cosmochimica Acta 57, 2227–2237.

Bebout, G.E., Ryan, J.G., Leeman, W.P., Bebout, A.E., 1999. Fractionation of trace elements by subduction-zone metamorphism – effect of convergent-margin thermal evolution. Earth and Planetary Science Letters 171, 63–81.

Benninghoven, A., Rüdenauer, F.G., Werner, H.W., 1987. Chemical Analysis, Bd. 86: Secondary Ion Mass Spectrometry: Basic Concepts, Instrumental Aspects, Applications and Trends. John Wiley and Sons, New York.

Benton, L.D., Ryan, J.G., Tera, F., 2001. Boron isotope systematics of slab fluids as inferred from a serpentine seamount, Mariana forearc. Earth and Planetary Science Letters 187, 273–282.

Benton, L.D., Ryan, J.G., Savov, I.P., 2004. Lithium abundance and isotope systematics of forearc serpentinites, Conical Seamount, Mariana forearc: Insights into the mechanics of slab-mantle exchange during subduction. Geochemistry, Geophysics, Geosystems 5.

Bloomer, S.H., Taylor, B., MacLeod, C.J., Stern, R.J., Fryer, P., Hawkins, J.W., Johnson, L., 1995. Early Arc volcanism and the Ophiolite problem: a perspective from drilling in the Western Pacific. In: Taylor, B., Natland, J. (Eds.), Active Margins and Marginal Basins of the Western Pacific. American Geophysical Union, Washington D.C., pp. 67–96.

Bonatti, E., Lawrence, J.R., Morandi, N., 1984. Serpentinization of oceanic peridotites: temperature dependence of mineralogy and boron content. Earth and Planetary Science Letters 70, 88–94.

Breeding, C.M., Ague, J.J., Brocker, M., 2004. Fluid-metasedimentary rock interactions in subduction-zone melange: implications for the chemical composition of arc magmas. Geology 32, 1041–1044.

Brown, E.H.T., 1977. The crossite content of Ca-amphibole as a guide to pressure of metamorphism. Journal of Petrology 18, 53–72.

Brown, E.H., Ghent, E.D., 1983. Mineralogy and phase relations in the blueschist facies of the Black Butte and Ball Rock areas, northern California Coast Ranges. American Mineralogist 68, 365–372.

Catanzaro, E.J., Champion, C.E., Garner, E.L., Malinenko, G., Sappenfeld, K.M., Shields, W.R., 1970. Boric acid, isotopic, and assay standard reference materials. National Bureau of Standards (U.S.), Special Publication, 260, pp. 17–70.

Chan, L.H., Leeman, W.P., You, C.F., 1999. Lithium isotopic composition of Central American Volcanic Arc lavas: implications for modification of subarc mantle by slab-derived fluids. Chemical Geology 160, 255–280.

Chan, L.H., Alt, J.C., Teagle, D.A.H., 2002. Lithium and lithium isotope profiles through the upper oceanic crust: a study of seawater-basalt exchange at ODP Sites 504B and 896A. Earth and Planetary Science Letters 201, 187–201.

Chaussidon, M., Jambon, A., 1994. Boron content and isotopic composition of oceanic basalts: geochemical and cosmochemical implications. Earth and Planetary Science Letters 121, 277–291.

Chaussidon, M., Marty, B., 1995. Primitive boron isotope composition of the mantle. Science 269, 383–386.

Cloos, M., 1986. Blueschists in the Franciscan Complex of California: petrotectonic constrains on uplift mechanism. Geological Society of America Memoir 164, 77–93.

Cloos, M., Shreve, R.L., 1996. Shear zone thickness and the seismicity of Chilean- and Mariana-type subduction zones. Geology 24, 107–110.

Coleman, R.G., Clark, J.R., 1968. Pyroxenes in the blueschist facies of California. American Journal of Science 266, 43–59.

Cosca, M.A., Arculus, R.J., Pearce, J.A., Mitchell, J.G., 1998. Ar-40/Ar-39 and K-Ar geochronological age constraints for the inception and early evolution of the Izu-Bonin-Mariana arc system. The Island Arc 7, 579–595.

Currie, L.A., 1968. Limits for qualitative detection and quantitative determination. Analytical Chemistry 40, 586–593.

Deschamps, F., Guillot, F., Godard, M., Andreani, M., Hattori, K., 2011. Serpentinites act as sponges for fluid-mobile elements in abyssal and subduction zone environments. Terra Nova 23, 171–178.

Domanik, K.J., Hervig, R.L., Peacock, S.M., 1993. Beryllium and boron in subduction zone minerals: an ion microprobe study. Geochimica et Cosmochimica Acta 57, 4997–5010.

Engdahl, E.R., van der Hilst, R., Buland, R., 1998. Global teleseismic earthquake relocation with improved travel times and procedures for depth determination. Bulletin of the Seismological Society of America 88, 722–743.

Essene, E.J., Fyfe, W.S., 1967. Omphacite in Californian metamorphic rocks. Contributions to Mineralogy and Petrology 15, 1–23.

Fisher, D.M., 1996. Fabrics and veins in the forearc: A record of cyclic fluid flow at depths of <15 km (Overview). In: Bebout, G.E., Scholl, D.W., Kirby, S.H., Platt, J. (Eds.), Subduction Top to Bottom: Geophysical Monograph, 96, pp. 75–89. Washington DC.

Foustoukos, D.I., Savov, I.P., Janecky, D.R., 2008. Chemical and isotopic constraints on water/rock interactions at the Lost City hydrothermal field, 30°N Mid-Atlantic Ridge. Geochimica et Cosmochimica Acta 72, 5457–5474.

Fryer, P.B., 1992. A synthesis of Leg 125 drilling of serpentine seamounts on the Mariana and Izu-Bonin forearcs. In: Fryer, P., Pearce, J.A., Stokking, L.B., et al. (Eds.), Proceedings to the Ocean Drilling Program, Scientific Results 125.

Fryer, P., Fryer, G.J., 1987. Origins of nonvolcanic seamounts in a forearc environment. In: Keating, B.H., Fryer, P., Batiza, R., Boehlert, G.W. (Eds.), Seamounts, Islands, and Atolls: Geophysical Monograph, 43, pp. 61–69.

Fryer, P., Hussong, D.M., 1982. Seafloor Spreading in the Mariana Trough: Results of Leg 60 Drill Site Selection Surveys. Initial Reports of the Deep Sea Drilling Project 60, 45–55.

Fryer, P., Mottl, M.J., 1992. Lithology, mineralogy, and origin of serpentine muds recovered from Conical and Torishima forearc seamounts: results of Leg 125 drilling. In:

Fryer, P., Pearce, J.A., Stokking, L.B., et al. (Eds.), Proceedings of the Ocean Drilling Program, Scientific Results, 125, pp. 343–362.
Fryer, P., Smoot, N.C., 1985. Processes of seamount subduction in the Mariana and Izu-Bonin trenches. Marine Geology 64, 77–90.
Fryer, P., Todd, C., 1999. Mariana blueschist mud volcanism sampling the subducted slab. Eos 80, 349.
Fryer, P.B., Salisbury, M.H., 2006. Leg 195 synthesis: Site 1200 - serpentinite seamounts of the Izu-Bonin/Mariana convergent plate margin (ODP Leg 125 and 195 drilling results). In: Shinohara, M., Salisbury, M.H., Richter, C. (Eds.), Proceedings of the Ocean Drilling Program, Scientific Results 195.
Fryer, P., Pearce, Julian A., Stokking, Laura B., et al., 1990. Bonin/Mariana region, covering Leg 125 of the cruises of the drilling vessel JOIDES Resolution, Apra Harbor, Guam, to Tokyo, Japan, sites 778–786. In: Fryer, P., Pearce, J.A., Stokking, L.B., et al. (Eds.), Proceedings of the Ocean Drilling Program Initial Reports, 125, pp. 367–380.
Fryer, P., Wheat, C.G., Mottl, M.J., 1999. Mariana blueschist mud volcanism: implications for conditions within the subduction zone. Geology 27, 103–106.
Fryer, P., Lockwood, J.P., Becker, N., Phipps, S., Todd, C.S., 2000. Significance of serpentine mud volcanism in convergent margins. Geological Society of America Special Papers 349, 35–51.
Fryer, P., Gharib, J., Ross, K., Savov, I., Mottl, M.J., 2006. Variability in serpentinite mudflow mechanisms and sources: ODP drilling results on Mariana forearc seamounts. Geochemistry, Geophysics, Geosystems 7.
Gharib, J., 2006. Clastic metabasites and authigenic minerals within serpentinite protrusions from the Mariana forearc: implications for sub-forearc subduction processes. PhD Dissertation, University of Hawaii.
Gharib, J.J., Fryer, P., Ross, K., 2002. Lithological and Mineralogical Analysis of Serpentine Mud Samples From the Mariana Forearc. American Geophysical Union, Fall Meeting 2002. abstract #T72A-1230.
Grove, M., Bebout, G.E., 1995. Cretacous tectonic evolution of coastal southern California: insights from the Catalina Schist. Tectonirc 14, 1290–1308.
Halama, R., Savov, I., Rudnick, R., McDonough, W., 2009. Insights into Li and Li isotope cycling and sub-arc metasomatism from veined mantle xenoliths, Kamchatka. Contributions to Mineralogy and Petrology 158, 197–222.
Horine, R.L., Moore, G.F., Taylor, B., 1990. Structure of the outer Izu-Bonin Forearc from seismic-reflection profiling and gravity modeling. In: Fryer, P., Pearce, J.A., Stokking, L.B., et al. (Eds.), Proceedings of the Ocean Drilling Program, Initial Reports, 125, pp. 81–94.
Hussong, D.M., Fryer, P., 1982. Structure and tectonics of the Mariana arc and forearc: drillsite selection surveys. Initial Reports of the Deep Sea Drilling Project 60, 33–44.
Ishikawa, T., Nakamura, E., 1992. Boron isotope geochemistry of the oceanic crust from DSDP/ODP Hole 504B. Geochimica et Cosmochimica Acta 56, 1633–1639.
Ishikawa, T., Nakamura, E., 1993. Boron isotope systematics of marine sediments. Earth and Planetary Science Letters 117, 567–580.
Ishikawa, T., Nakamura, E., 1994. Origin of the slab component in arc lavas from across-arc variation of B and Pb isotopes. Nature 370, 205–208.
Ishikawa, T., Tera, F., 1997. Source, composition and distribution of the fluid in the Kurile mantle wedge: constraints from across-arc variations of B/Nb and B isotopes. Earth and Planetary Science Letters 152, 123–138.
Ishikawa, T., Tera, F., 1999. Two isotopically distinct fluid components involved in the Mariana arc: evidence from Nb/B ratios and B, Sr, Nd, and Pb isotope systematics. Geology 27, 83–86.
Johnson, L.E., 1992. Mafic clasts in serpentine seamounts: petrology and geochemistry of a diverse crustal suite from the outer Mariana forearc. In: Fryer, P., Pearce, J.A., Stokking, L.B., et al. (Eds.), Proceedings of the Ocean Drilling Program, Scientific Results, 125, pp. 401–413.
Johnson, L.E., Fryer, P., 1990. The first evidence for MORB-like lavas from the outer Mariana forearc: geochemistry, petrography and tectonic implications. Earth and Planetary Science Letters 100, 304–316.
Kastner, M., Elderfield, H., 1993. Data report: compositions of fluids and authigenic phases in sediments of the Nankai Trough accretionary complex. In: Hill, I.A., Taira, A., Firth, J.V., et al. (Eds.), Proceedings of the Ocean Drilling Program, Scientific Results, 131, pp. 423–425.
Kastner, M., Elderfield, H., Jenkins, W.J., Gieskes, J.M., Gamo, T., 1993. Geochemical and isotopic evidence for fluid flow in the western Nankai subduction zone, Japan. In: Hill, I.A., Taira, A., Firth, J.V., et al. (Eds.), Proceedings of the Ocean Drilling Program, Scientific Results, 131, pp. 397–413.
Kelley, K.A., Plank, T., Ludden, J., Staudigel, H., 2003. Composition of altered oceanic crust at ODP Sites 801 and 1149. Geochemistry, Geophysics, Geosystems 4.
King, R.L., Kohn, M.J., Eiler, J.M., 2003. Constraints on the petrologic structure of the subduction zone slab–mantle interface from Franciscan Complex exotic ultramafic blocks. Geological Society of America Bulletin 115, 1097–1109.
King, R.L., Bebout, G.E., Moriguti, T., Nakamura, E., 2006. Elemental mixing systematics and Sr-Nd isotope geochemistry of melange formation: Obstacles to identification of fluid sources to arc volcanics. Earth and Planetary Science Letters 246, 288–304.
King, R.L., Bebout, G.E., Grove, M., Moriguti, T., Nakamura, E., 2007. Boron and lead isotope signatures of subduction-zone mélange formation: hybridization and fractionation along the slab–mantle interface beneath volcanic arcs. Chemical Geology 239, 305–322.
Kodolányi, J., Pettke, T., 2011. Loss of trace elements from serpentinites during fluid-assisted transformation of chrysotile to antigorite – an example from Guatemala. Chemical Geology 284, 351–362.
Kretz, R., 1983. Symbols for rock-forming minerals. American Mineralogist 68, 277–279.
Lagabrielle, Y., Karpoff, A.-M., Cotten, J., 1992. Mineralogical and geochemical analysis of sedimentary serpentinites from Conical Seamount (Hole 778A): implication for the evolution of serpentine seamounts. In: Fryer, P., Pearce, J.A., Stokking, L.B., et al. (Eds.), Proceedings of the Ocean Drilling Program, Scientific Results, 125, pp. 325–342.
Leeman, W., 1996. Boron and other fluid-mobile elements in volcanic arc lavas: implications for subduction processes. Geophysical Monograph Series 96, 269–276.
Leeman, W.P., Sisson, V.B., 2002. Geochemistry of boron and its implications for crustal and mantle processes, In: Grew, E.S., Anovitz, L.M. (Eds.), Boron: Mineralogy, Petrology and Geochemistry, 2nd edn. Mineral. Soc. Am., Washington, DC, pp. 645–708.
Lyubetskaya, T., Korenaga, J., 2007. Chemical composition of Earth's primitive mantle and its variance: 1. Method and results. Journal of Geophysical Research-Solid Earth 112 (B3).
Maekawa, H., 1995. Metamorphic rocks from serpentinite seamounts in the Mariana and Izu-Bonin forearcs. In: Tokuyama, H., Shecheka, S.A., Isezaki, N., et al. (Eds.), Geology and Geophysics of the Philippine Sea. Terra Scientific Publishing Company, Tokyo, pp. 357–369.
Maekawa, H., Shozui, M., Ishii, T., Saboda, K.L., Ogawa, Y., 1992. Metamorphic rocks from the serpentinite seamounts in the Mariana and Izu-Ogasawara forearcs. In: Fryer, P., Pearce, J.A., Stokking, L.B., et al. (Eds.), Proceedings of the Ocean Drilling Program, Scientific Results, 125, pp. 415–430.
Maekawa, H., Shozui, M., Ishii, T., Fryer, P., Pearce, J.A., 1993. Blueschist metamorphism in an active subduction zone. Nature 364, 520–523.
Manning, C.E., 1997. Coupled reaction and flow in subduction zones: silica metasomatism in the mantle wedge. In: Jamtveit, B., Yardley, B.W.D. (Eds.), Fluid flow and transport in rocks: mechanisms and effects. Chapman & Hall, London, pp. 139–148.
Marschall, H.R., 2005. Lithium, beryllium and boron in high-pressure metamorphic rocks from Syros (Greece). Mathematisch-Naturwissenschaftlichen Gesamtfakultät. Ruprecht-Karls-Universität, Heidelberg, Germany.
Marschall, H.R., Ludwig, T., 2004. The low-boron contest: minimising surface contamination and analysing boron concentrations at the ng/g-level by secondary ion mass spectrometry. Mineralogy and Petrology 81, 265–278.
Marschall, H.R., Altherr, R., Ludwig, T., Kalt, A., Gméling, K., Kasztovszky, Z., 2006a. Partitioning and budget of Li, Be and B in high-pressure metamorphic rocks. Geochimica et Cosmochimica Acta 70, 4750–4769.
Marschall, H.R., Ludwig, T., Altherr, R., Kalt, A., Tonarini, S., 2006b. Syros metasomatic tourmaline: evidence for very high-delta B-11 fluids in subduction zones. Journal of Petrology 47, 1915–1942.
Marschall, H.R., Altherr, R., Rüpke, L., 2007. Squeezing out the slab – modelling the release of Li, Be and B during progressive high-pressure metamorphism. Chemical Geology 239, 323–335.
Miller, D.P., Marschall, H.R., Schumacher, J.C., 2009. Metasomatic formation and petrology of blueschist-facies hybrid rocks from Syros (Greece): implications for reactions at the slab–mantle interface. Lithos 107, 53–67.
Moran, A.E., Sisson, V.B., Leeman, W.P., 1992. Boron depletion during progressive metamorphism: implications for subduction processes. Earth and Planetary Science Letters 111, 331–349.
Moriguti, T., Nakamura, E., 1998. High-yield lithium separation and the precise isotopic analysis for natural rock and aqueous samples. Chemical Geology 145, 91–104.
Mottl, M.J., 1983. Metabasalts, axial hot springs, and the structure of hydrothermal systems at mid-ocean ridges. Geological Society of America Bulletin 94, 161–180.
Mottl, M.J., Wheat, G., Baker, E., Becker, N., Davis, E., Feely, R., Grehan, A., Kadko, D., Lilley, M., Massoth, G., Moyer, C., Sansone, F.T., 1998. Warm springs discovered on 3.5 Ma oceanic crust, eastern flank of the Juan de Fuca Ridge. Geology 26.
Mottl, M.J., Komor, S.C., Fryer, P., Moyer, C.L., 2003. Deep-slab fuel extremophilic Archaea on a Mariana forearc serpentinite mud volcano: Ocean Drilling Program Leg 195. Geochemistry, Geophysics, Geosystems 4.
Mottl, M.J., Wheat, C.G., Fryer, P., Gharib, J., Martin, J.B., 2004. Chemistry of springs across the Mariana forearc shows progressive devolatilization of the subducting plate. Geochimica et Cosmochimica Acta 68, 4915–4933.
Nakano, T., Nakamura, E., 2001. Boron isotope geochemistry of metasedimentary rocks and tourmalines in a subduction zone metamorphic suite. Physics of the Earth and Planetary Interiors 127, 233–252.
Oakley, A.J., Taylor, B., Moore, G.F., 2008. Pacific Plate subduction beneath the central Mariana and Izu-Bonin fore arcs: New insights from an old margin. Geochemistry, Geophysics, Geosystems 9.
Ottolini, L., Bottazzi, P., Vannucci, R., 1993. Quantification of lithium, beryllium, and boron in silicates by secondary-ion mass-spectrometry using conventional energy-filtering. Analytical Chemistry 65, 1960–1968.
Pabst, S., 2009. Investigation of blueschist and serpentinized harzburgite from the Mariana forearc: Insights into the mechanisms of element mobilization in subduction zones and storage of fluid-mobile elements in the mantle wedge. PhD Dissertation, Heidelberg, Germany. http://www.ub.uni-heidelberg.de/archiv/10181.
Pabst, S., Zack, T., Savov, I.P., Ludwig, T., Rost, D., Vicenzi, E.P., 2011. Evidence for boron incorporation into the serpentine crystal structure. American Mineralogist 96, 1112–1119.
Palmer, M.R., 1991. Boron-isotope systematics of Halmahera arc (Indonesia) lavas: evidence for involvement of the subducted slab. Geology 19, 215–217.
Palmer, M.R., Swihart, G.H., 1996. Boron isotope geochemistry: an overview. In: Grew, E.S., Anovitz, I.M. (Eds.), Boron: Mineralogy, Petrology and Geochemistry: Reviews in Mineralogy, 33, pp. 709–744.
Peacock, S.M., Hervig, R.L., 1999. Boron isotopic composition of subduction-zone metamorphic rocks. Chemical Geology 160, 281–290.
Peacock, S.M., Hyndman, R.D., 1999. Hydrous minerals in the mantle wedge and the maximum depth of subduction thrust earthquakes. Geophysical Research Letters 26, 2517–2520.
Pearce, N.J.G., Perkins, W.T., Westgate, J.A., Gorton, M.P., Jackson, S.E., Neal, C.R., Chenery, S.P., 1997. A compilation of new and published major and trace element data for

NIST SRM 610 and NIST SRM 612 glass reference materials. Geostandards Newsletter-the Journal of Geostandards and Geoanalysis 21, 115–144.
Pelletier, L., Vils, F., Kalt, A., Gmeling, K., 2008. Li, B and Be Contents of Harzburgites from the Dramala Complex (Pindos Ophiolite, Greece): Evidence for a MOR-type Mantle in a Supra-subduction Zone Environment. Petrology 57.
Reinen, L.A., 2000. Seismic and aseismic slip indicators in serpentinite gouge. Geology 28, 135–138.
Reinen, L.A., Weeks, J.D., Tullis, T.E., 1994. The frictional behavior of lizardite and antigorite serpentinites: experiments, constitutive models, and implications for natural faults. Pure and Applied Geophysics 143, 317–358.
Rose, E.F., Shimizu, N., Layne, G.D., Grove, T.L., 2001. Melt production beneath Mt. Shasta from boron data in primitive melt inclusions. Science 293, 281–283.
Rosner, M., Erzinger, J., Franz, G., Trumbull, R.B., 2003. Slab-derived boron isotope signatures in arc volcanic rocks from the Central Andes and evidence for boron isotope fractionation during progressive slab dehydration. Geochemistry, Geophysics, Geosystems 4.
Rosner, M., Wiedenbeck, M., Ludwig, T., 2008. Composition-induced variations in SIMS instrumental mass fractionation during boron isotope ratio measurements of silicate glasses. Geostandards and Geoanalytical Research 32, 27–38.
Ryan, J.G., 2002. Trace-elements systematics of beryllium in terrestrial materials. In: Grew, E.S. (Ed.), Beryllium: mineralogy, petrology and geochemistry: Reviews in Mineralogy and Geochemistry, 50, pp. 121–145.
Ryan, J.G., Langmuir, C.H., 1987. The systematics of lithium abundances in young volcanic rocks. Geochimica et Cosmochimica Acta 51, 1727–1741.
Ryan, J.G., Langmuir, C.H., 1988. Beryllium systematics in young volcanic-rocks – implications for Be-10. Geochimica et Cosmochimica Acta 52, 237–244.
Ryan, J.G., Langmuir, C.H., 1993. The systematic of boron abundances in young volcanic-rocks. Geochimica et Cosmochimica Acta 57, 1489–1498.
Ryan, J.G., Morris, J., Tera, F., Leeman, W.P., Tsvetkov, A., 1995. Cross-arc geochemical variations in the Kurile-arc as a function of slab depth. Science 270, 625–627.
Ryan, J.G., Leeman, W.P., Morris, J.D., Langmuir, C.H., 1996. The boron systematics of intraplate lavas: implications for crustal and mantle evolution. Geochimica et Cosmochimica Acta 60, 415–422.
Salisbury, M.H., Shinohara, M., Richter, C., Araki, E., Barr, S.R., D'Antonio, M., Dean, S.M., Diekmann, B., Edwards, K.M., Fryer, P.B., Gaillot, P.J., Hammon III, W.S., Hart, D., Januszczak, N., Komor, S.C., Kristensen, M.B., Lockwood, J.P., Mottl, M.J., Moyer, C.L., Nakahigashi, K., Savov, I.P., Su, X., Wei, K.-Y., Yamada, T., 2002. Proceeding of the Ocean Drilling Program, Initial Reports, 195.
Salters, V.J.M., Stracke, A., 2004. Composition of the depleted mantle. Geochemistry, Geophysics, Geosystems 5, Q05004.
Sample, J.C., Karig, D.E., 1982. A volcanic production rate for the Mariana island arc. Journal of Volcanology and Geothermal Research 13, 73–82.
Sano, S., Offler, R., Hyodo, H., Watanabe, T., 2004. Geochemistry and chronology of tectonic blocks in serpentinite mèlange of the Southern New England Fold Belt, NSW, Australia. Gondwana Research 7, 817–831.
Sano, T., Miyoshi, M., Ingle, S., Banerjee, N.R., Ishimoto, M., Fukuoka, T., 2008. Boron and chlorine contents of upper oceanic crust: Basement samples from IODP Hole 1256D. Geochemistry, Geophysics, Geosystems 9, Q12O15.
Savov, I.P., Tonarini, S., Ryan, J., Mottl, M., 2004. Boron isotope geochemistry of serpentinites and porefluids from Leg 195, Site 1200, S.Chamorro Seamount, Mariana forearc region. International Geological Congress (IGC), Florence, Italy.
Savov, I.P., Guggino, S., Ryan, J.G., Fryer, P., Mottl, M.J., 2005a. Geochemistry of serpentinite muds and metamorphic rocks from the Mariana forearc, ODP Sites 1200 and 778–779, South Chamorro and Conical Seamounts. In: Shinohara, M., Salisbury, M.H., Richter, C. (Eds.), Proceedings of the Ocean Drilling Program, Scientific Results, 195.
Savov, I.P., Ryan, J.G., D'Antonio, M., Kelley, K., Mattie, P., 2005b. Geochemistry of serpentinized peridotites from the Mariana Forearc Conical Seamount, ODP Leg 125: Implications for the elemental recycling at subduction zones. Geochemistry, Geophysics, Geosystems 6.
Savov, I.P., Ryan, J.G., D'Antonio, M., Fryer, P., 2007. Shallow slab fluid release across and along the Mariana arc-basin system: insights from geochemistry of serpentinized peridotites from the Mariana fore arc. Journal of Geophysical Research 112, B09205.
Savov, I.P., Leeman, W.P., Lee, C.T., Shirey, S.B., 2009. Boron isotope variations in NW USA rhyolites-E.Oregon, Snake River Plain, Yellowstone. Journal of Volcanology and Geothermal Research 188, 162–172.
Scholz, C.H., Small, C., 1997. The effect of seamount subduction on seismic coupling. Geology 25, 487–490.
Seno, T., Maruyama, S., 1984. Paleogeographic reconstruction and origin of the Philippine Sea. Tectonophysics 102, 53–84.
Seno, T., Stein, S., Gripp, A.E., 1993. A Model for the Motion of the Philippine Sea Plate Consistent With NUVEL-1 and Geological Data. Geophysical Research 98.
Shipley, T.H., McIntosh, K.D., Silver, E.A., Stoffa, P.L., 1992. Three-Dimensional Seismic Imaging of the Costa Rica Accretionary Prism: Structural Diversity in a Small Volume of the Lower Slope. Journal of Geophysical Research 97.
Smith, H.J., Spivack, A.J., Staudigel, H., Hart, S.R., 1995. The boron isotopic composition of altered oceanic crust. Chemical Geology 126, 119–135.
Smith, H.J., Leeman, W.P., Davidson, J., Spivack, A.J., 1997. The B isotopic composition of arc lavas from Martinique, Lesser Antilles. Earth and Planetary Science Letters 146, 303–314.
Snyder, G.T., Savov, I.P., Muramatsu, Y., 2005. Iodine and boron in Mariana serpentinite mud volcanoes (ODP Legs 125 and 195): implications for forearc processes and subduction recycling. In: Shinohara, M., Salisbury, M.H., Richter, C. (Eds.), Proceedings of the Ocean Drilling Program, Scientific Results, 195.
Sorensen, S.S., Grossman, J.N., 1989. Enrichment of trace-elements in garnet amphibolites from a Paleo-subduction zone-Catalina schist, Southern California. Geochimica et Cosmochimica Acta 53, 3155–3177.
Spivack, A.J., Palmer, M.R., Edmond, J.M., 1987. The sedimentary cycle of the boron isotopes. Geochimica et Cosmochimica Acta 51, 1939–1949.
Stephan, T., 2001. TOF-SIMS in cosmochemistry. Planetary and Space Science 49, 859–906.
Stern, R.J., Bloomer, S.H., 1992. Subduction zone infancy: examples from the Eocene Izu-Bonin-Mariana and Jurassic California arcs. Geological Society of America Bulletin 104, 1621–1636.
Stern, R.J., Fouch, M.J., Klemperer, S., 2003. An overview of the Izu-Bonin-Mariana subduction factory. Geophysical Monograph Series 138, 175–223.
Straub, S.M., Layne, G.D., 2002. The systematics of boron isotopes in Izu arc front volcanic rocks. Earth and Planetary Science Letters 198, 25–39.
Tatsumi, Y., Hamilton, D.L., Nesbitt, R.W., 1986. Chemical characteristics of fluid phase released from a subducted lithosphere and origin of arc magmas: evidence from high-pressure experiments and natural rocks. Journal of Volcanology and Geothermal Research 29, 293–309.
Thompson, G., Melson, W.G., 1970. Boron contents of serpentinites and metabasalts in the oceanic crust: Implications for the boron cycle in the oceans. Earth and Planetary Science Letters 8, 61–65.
Tomascak, P.B., Widom, E., Benton, L.D., Goldstein, S.L., Ryan, J.G., 2002. The control of lithium budgets in island arcs. Earth and Planetary Science Letters 196, 227–238.
Tonarini, S., Armienti, P., D'Orazio, M., Innocenti, F., 2001. Subduction-like fluids in the genesis of Mt. Etna magmas: evidence from boron isotopes and fluid mobile elements. Earth and Planetary Science Letters 192, 471–483.
Tonarini, S., Pennisi, M., Adorni-Braccesi, A., Dini, A., Ferrara, G., Gonfiantini, R., Wiedenbeck, M., Gröning, M., 2003. Intercomparison of boron isotope and concentration measurements. Part I: Selection, preparation and homogeneity tests of the intercomparison materials. Geostandards Newsletter 26, 21–39.
Tonarini, S., Agostini, S., Doglioni, C., Innocenti, F., Manetti, P., 2007. Evidence for serpentinite fluid in convergent margin systems: the example of El Salvador (Central America) arc lavas. Geochemistry, Geophysics, Geosystems 8, Q09014.
Tonarini, S., Leeman, W.P., Leat, P.T., 2011. Subduction erosion of forearc mantle wedge implicated in the genesis of the South Sandwich Island (SSI) arc: evidence from boron isotope systematics. Earth and Planetary Science Letters 301, 275–284.
Underwood, M.B., Yu'suke Kubo, S.S., the IODP Expedition 322 Scientists, 2010. IODP Expedition 322 Drills Two Sites to Document Inputs to The Nankai Trough Subduction Zone. Scientific Drilling 10, 14–25.
Uyeda, S., 1982. Subduction zones: an introduction to comparative subductology. Tectonophysics 81, 133–159.
Uyeda, S., Kanamori, H., 1979. Back-arc opening and the mode of subduction. Journal of Geophysical Research 84, 1049–1061.
Vils, F., Pelletier, L., Kalt, A., Müntener, O., Ludwig, T., 2008. The lithium, boron and beryllium content of serpentinized peridotites from ODP Leg 209 (Sites 1272A and 1274A): implications for lithium and boron budgets of oceanic lithosphere. Geochimica et Cosmochimica Acta 72, 5475–5504.
Vils, F., Tonarini, S., Kalt, A., Seitz, H.-M., 2009. Boron, lithium and strontium isotopes as tracers of seawater-serpentinite interaction at Mid-Atlantic ridge, ODP Leg 209. Earth and Planetary Science Letters 286, 414–425.
Vils, F., Müntener, O., Kalt, A., Ludwig, T., 2011. Implications of the serpentine phase transition on the behaviour of beryllium and lithium-boron of subducted ultramafic rocks. Geochimica et Cosmochimica Acta 75, 1249–1271.
Williams, L.B., Wieser, M.E., Fennell, J., Hutcheon, I., Hervig, R.L., 2001. Application of boron isotopes to the understanding of fluidrock interactions in a hydrothermally stimulated oil reservoir in the Alberta Basin, Canada. Geofluids 1, 229–240.
Wunder, B., Meixner, A., Romer, R.L., Wirth, R., Heinrich, W., 2005. The geochemical cycle of boron: constraints from boron isotope partitioning experiments between mica and fluid. Lithos 84, 206–216.
Yamazaki, T., Okamura, Y., 1989. Subducting seamounts and deformation of overriding forearc wedges around Japan. Tectonophysics 160, 207–229.
You, C.-F., Gieskes, J.M., Chen, R.F., Spivack, A., Gamo, T., 1993. Iodide, bromide, manganese, boron, and dissolved organic carbon in interstitial waters of the organic carbon–rich marine sediments: observations in the Nankai accretionary prism. In: Hill, I.A., Taira, A., Firth, J.V., et al. (Eds.), Proceedings of the Ocean Drilling Program,Scientific Results, 131, pp. 165–174.
You, C.F., Spivack, A.J., Gieskes, J.M., Rosenbauer, R., Bischoff, J.L., 1995. Experimental study of boron geochemistry: implications for fluid processes in subduction zones. Geochimica et Cosmochimica Acta 59, 2435–2442.
Zack, T., Tomascak, P.B., Rudnick, R.L., Dalpé, C., McDonough, W.F., 2003. Extremely light Li in orogenic eclogites: the role of isotope fractionation during dehydration in subducted oceanic crust. Earth and Planetary Science Letters 208, 279–290.